

The estimates of carbon sequestration potential in an expanding Arctic fjord affected by dark plumes of glacial meltwater (Hornsund, Svalbard)

Marlena Szeligowska¹, Déborah Benkort², Anna Przyborska³, Mateusz Moskalik⁴, Bernabé Moreno¹,
5 Emilia Trudnowska¹, Katarzyna Błachowiak-Samołyk¹

¹Marine Ecology Department, Institute of Oceanology, Polish Academy of Sciences, Sopot, 81-712, Poland

²Institute of Coastal Systems - Analysis and Modeling, Helmholtz-Zentrum Hereon, Geesthacht, 21502, Germany

³Physical Oceanography Department, Institute of Oceanology, Polish Academy of Sciences, Sopot, 81-712, Poland

⁴Department of Polar and Marine Research, Institute of Geophysics, Polish Academy of Sciences, Warsaw, 01-452, Poland

10 *Correspondence to:* Marlena Szeligowska (lena@iopan.pl)

Abstract. In polar regions, glaciers are retreating onto land, gradually widening ice-free coastal waters which are known to act as new sinks of atmospheric carbon. However, the increasing delivery of inorganic suspended particulate matter (iSPM) with meltwater might significantly impact their capacity to contribute to carbon sequestration. Here, we present an analysis of satellite, meteorological, and SPM data as well as results of the coupled physical-biogeochemical model (1D GOTM-
15 ECOSMO-E2E-Polar) with the newly implemented iSPM group, to show its impact on the ecosystem dynamics in a warming polar fjord (Hornsund, European Arctic). Our results indicate that with a longer melt season (9 days per decade, 1979-2022), decreased sea ice duration (44 days per decade, 1982-2021) and formation of new marine habitats after the retreat of marine-terminating glaciers (around 100 km² in 1976-2022, 38% increase in the total area), glacial meltwater has transported increasing loads of iSPM from land (3.7 g·m⁻³ per decade, reconstructed for 1979-2022). The simulated light limitation induced
20 by iSPM input delayed and decreased phytoplankton, zooplankton, and macrobenthos peak occurrences. The newly ice-free areas still markedly contributed to the plankton primary and secondary production, and carbon burial in sediments (5.1, 2.0, and 0.9 GgC per year, respectively, average for 2005-2009 in the iSPM scenario). However, these values would have been higher by 5.0, 2.1 and 0.1 GgC per year, respectively, without iSPM input. Since carbon burial was the least affected by iSPM (around 16% decrease in comparison to 50% for plankton primary and secondary production), the impact of marine ice loss
25 and enhanced land-ocean connectivity should be further investigated in the context of carbon fluxes in expanding polar fjords.

1 1 Introduction

Organic carbon burial in marine sediments represents the dominant natural pathway toward long-term sequestration and hence plays a key role in controlling atmospheric O₂ and CO₂ concentrations (Bernier, 1982; Hedges and Keil, 1995). While important carbon sinks at coastal wetlands (mangroves forests, salt marshes, and seagrass beds) are declining globally (Duarte et al.,
30 2005; Howard et al., 2014), new marine habitats are opening up in the Arctic and West Antarctic due to glaciers retreat and

giant iceberg calving (Ficetola et al., 2021). Within these newly formed coastal ecosystems, CO₂ drawdown by phytoplankton and ice algae is supported by nutrient input from land intensifying the cascade from carbon capture into storage and burial in sediments (Ardyna and Arrigo, 2020; Arrigo et al., 2008; Wadham et al., 2019). Due to the high sedimentation rates, emerging and expanding fjords play an important role as efficient carbon burial hot spots (Bianchi et al., 2020; Cui et al., 2022; Smith et al., 2015). Thus, the loss of marine ice in polar coastal waters might, to some extent, compensate for decreasing coastal carbon sinks elsewhere (Barnes, 2017; Peck et al., 2010; Zwerschke et al., 2022).

Despite recent increases in primary and secondary production due to, among others, the earlier break-up of seasonal sea ice, the polar regions' potential for long-term carbon burial in sediments is ultimately limited by multifarious mechanisms. The changes in the duration and composition of ice algae blooms weaken the sympagic-benthic coupling, in consequence leaving more biomass that can be utilized and dispersed in the pelagic system (Fadeev et al., 2021; Lalande et al., 2019; Riser et al., 2008). Thus, warming induces the maturation of polar fjords through the transition to a more complex but effective pelagic food web that consumes most of the available organic matter, and thus leaving less carbon to be deposited at the bottom (Węśławski et al., 2017; Zaborska et al., 2018). Furthermore, the delivery of inorganic suspended particulate matter (iSPM) with glacial meltwater dims underwater light later in the productive season (summer and autumn) (Szeligowska et al., 2022) and results in a significant reduction of phytoplankton and phyto-benthos biomass (Blain et al., 2021; Deregibus et al., 2016; Holt et al., 2016) that influences carbon burial potential in glacial bays.

Further warming will likely exacerbate sediment input through increasing precipitation, erosion enhanced by storm activity, glacial melt, permafrost thaw, and sea-level rise (Syvitski et al., 2005, 2022). Moreover, in situ observations and numerical simulations in arctic fjords suggest that after marine-terminating glaciers retreat onto land, subglacial discharge and nutrients upwelling ceases, enhancing surface stratification and weakening vertical mixing, therefore reducing the productivity in coastal zones (Hopwood et al., 2018; Meire et al., 2017). However, our understanding of the rapid transformations of polar marine ecosystems in response to climatic stressors remains insufficient due to, among others, the scarcity of long-term standardized monitoring data (Schofield et al., 2010). While numerical models were essential in filling the knowledge gaps related to the mechanisms of nutrient supply with meltwater (Castelao et al., 2019; Oliver et al., 2020) and substantial effort has been put into incorporating modules representing biogeochemistry in sea ice (Steiner et al., 2016), only few of them resolve inorganic particulate matter dynamics in glacier-fed basins (Neder et al., 2022). So far, these models do not typically represent the impact of the delivery of terrigenous material on biological production and carbon budgets.

This study aimed to assess the gains and losses in plankton primary and secondary production, and carbon burial due to the transformations of the coastal waters in the European Arctic. We investigated Hornsund (Svalbard, West Spitsbergen) as a model high-latitude fjord, since it is among the best studied fjords in the Arctic and represents an area of rapid regional warming with many bays affected by the recession of glaciers. Thus, here we (1) map the extent of emerging habitat after the retreat of marine-terminating glaciers and (2) simulate how the ecosystem dynamics and carbon sequestration are affected by sediment discharge in these bays using a 1D coupled physical-biogeochemical model (GOTM-ECOSMO-E2E-Polar) with a newly implemented iSPM group. We present the results of our simulations for 2005-2009, i.e., a period with an exceptionally strong

65 warming signal (Muckenhuber et al., 2016; Promińska et al., 2017) in the context of multidecadal (1976-2022) changes in the physical environment, to discuss the potential of newly ice-free areas to act as emerging carbon sinks and their role in the global carbon cycle.

2 Methods

2.1 Study area

70 Hornsund is a glaciomarine fjord of Svalbard with inner basins affected by glacial outflow (Fig. 1) (Błaszczuk et al., 2019). Since the strong polar front formed by the West Spitsbergen Current (saline and warm Atlantic Water) and the Sørkapp Current (cold and relatively fresh Arctic Water) reduces the advection of Atlantic Water into Hornsund in comparison to other West Spitsbergen fjords (Promińska et al., 2017), it is considered a less mature, highly productive cold-water fjord with an Arctic-type resident biota and relatively high sequestration of organic carbon (Węśławski et al., 2017; Zaborska et al., 2018).
75 Characterized by dynamic paraglacial coastal systems with high sediment mobility, Brepollen is the most extensive bay in Hornsund, where >85 km of new shoreline was formed in the last century after an ice retreat (Strzelecki et al., 2020). The area is known for one of the fastest retreat rates of marine-terminating glaciers in the Svalbard archipelago, which has accelerated in this century up to around 3 km² per year in 2001-2010 (Błaszczuk et al., 2013). Importantly, the ice bridge between Brepollen and Hambergbukta (Fig. 1b, currently <5km wide) is predicted to break up in the coming decades (Grabiec et al., 2018; Osika
80 et al., 2022), thus reopening a direct connection to the Barents Sea and changing the hydrodynamic conditions for biological production and carbon burial by either stronger sea ice or Atlantic Water advection.

2.2 Datasets

2.2.1 The area and volume of newly ice-free marine habitats

Summertime Landsat images of Hornsund were downloaded from <https://glovis.usgs.gov/app> (Sup. Tab. 1). Only cloud-free
85 images with no sea ice cover (from July to early September) were used. When present, 4-3-2 and 3-2-1 spectral bands (Landsat 8 and Landsat 1-7, respectively) were used to prepare RGB composites, and a panchromatic band (8) was used to enhance the resolution. Newly ice-free areas were manually delineated with the position of glacier fronts in 1976 as a reference since it was the first year with Landsat images available in summer (Fig. 1b). The same person (MS) repeated the procedure three times for each year to test the repeatability of manual digitisation. The standard deviation was up to 0.23 km². Importantly, the
90 fronts of marine-terminating glaciers undergo seasonal fluctuations, which might increase uncertainty (Błaszczuk et al., 2021, 2023) thus, the analysis was narrowed to the main melt season (from July to early September). Marine habitat volume was calculated based on digitized area and bathymetry data from Hornsund (grid size 100 m) (Moskalik et al., 2014) using the zonal statistics method in ArcGIS Pro 2.8.0. Marine habitat volume was calculated until 2010, since the bathymetric data were not available for the glacial bays that emerged after 2010.

95 **2.2.2 Sea/ice surface temperature and sea ice concentration**

Sea and ice surface temperature (SST) and sea-ice concentration (SIC) variables were extracted from the Arctic Sea and Ice Surface Temperature dataset (L4, 5km, daily). These data were provided by Danish Meteorological Institute and MyOcean regional data assembly centre and created using multisensor satellite surface temperature observations. Since the dataset did not cover all the fjord, data were extracted from points in the outer/central parts (Fig. 1, Sup. Tab. 2) assuming that they reflect the SST/SIC conditions in the inner fjord. This assumption is supported by previous studies (Arntsen et al., 2019; Błaszczyk et al., 2021; Sutherland et al., 2013) and the fact that this analysis focuses on relative changes in melt season intensity rather than absolute values. The data were extracted for three adjacent cells (Sup. Tab. 2) and averaged. Sea ice-free days (SIF) were defined as a fraction of the year with SIC<15%. The monthly mean extent of SIC>15% in March 2005 and 2006 is shown in Fig. 1a. The sum of all daily SST>0°C (positive degree days, PDD SST) was calculated for each year (annual) and each melt season (summertime, June-August) as a proxy for submarine melt potential (Luckman et al., 2015; Błaszczyk et al., 2021, 2023).

2.2.3 Air temperature and precipitation

Air temperature and precipitation datasets from Polish Polar Station Hornsund (PPS, Fig. 1c) were downloaded from Wawrzyniak and Osuch (2020) (1979-2018, <https://doi.pangaea.de/10.1594/PANGAEA.909042>) and from SIOS (110 <https://doi.org/10.5194/essd-12-805-2020>, 2018-2022). Daily average air temperature (AT) was used to calculate the sum of all daily AT>0°C (PDD AT) for each year (annual) and each melt season (summertime, June-August) as a proxy for surface melt potential (Hock, 2005; Rignot et al., 2008). Annual and summertime (June-August) precipitation was calculated by summing up the daily precipitation measurements (mm). The start of the melt season was defined as the start of the first period of six consecutive days with AT>0°C; similarly, the end of the melt season was defined as the first of six consecutive days (115 with AT<0°C (modified from Błaszczyk et al., 2021). This definition considers the delays in meltwater and particulate matter delivery to the fjord and the 6-days window was shown to be well correlated with sediment flux (this study and D'Angelo et al., 2018). Melt season duration was calculated as the number of days between the end and the start of the melt season and provided as a fraction of the year.

2.2.4 Suspended particulate matter, sediment flux, and salinity

120 Datasets for suspended particulate matter (SPM), sediment flux, and salinity collected in Hansbukta (2015-2021) at long-term monitoring stations (Fig. 1c, Sup. Tab. 2) were downloaded from <https://dataportal.igf.edu.pl/group/longhorn> (see detailed description in Moskalik et al., 2018). In this study, sediment flux data from sediment traps deployed for one day at 5, 10, 15, and 20 m depth were considered for analysis. Inorganic and organic SPM concentration ($\text{g}\cdot\text{m}^{-3}$) and sediment flux ($\text{g}\cdot\text{m}^{-2}\cdot\text{day}^{-1}$) were calculated based on total SPM/sediment flux and the loss on ignition (Moskalik et al., 2018). Integrated iSPM (125 concentration in the water column was averaged for the main melt season (June-August, 2016-2021). The annual variability

in the SPM levels was visualized using a kernel density estimate (KDE) plot prepared based on SPM data (2015–2021) from discrete depths. The sinking rate of SPM ($\text{m}\cdot\text{day}^{-1}$) was calculated by dividing sediment flux by SPM concentration sampled at corresponding depth layers (Mugford and Dowdeswell, 2011). Sediment flux and salinity datasets were used for model parametrisation (see 2.3.1), whereas the SPM dataset was used for model assessment (see 2.4).

130 2.3 Numerical model

To study the dynamics of West Spitsbergen coastal waters affected by iSPM input, numerical experiments were designed using the polar version of the biogeochemical ECOSystem Model (ECOSMO-E2E-Polar version) coupled with the General Ocean Turbulence Model (GOTM) (Burchard et al., 1999). ECOSMO-E2E-Polar version represents the three main nutrient cycles (nitrogen, phosphorus, and silica) in the pelagic and sympagic systems, three functional groups of primary producers (ice algae, 135 diatoms, and flagellates), two zooplankton groups (micro- and meso-), one macrobenthos group, and chlorophyll *a* as a prognostic variable allowing a flexible chlorophyll-to-carbon ratio. The ECOSMO developments are fully described in Benkort et al. (2020), Daewel et al. (2018), Daewel and Schrum (2013), Yumruktepe et al. (2022). We extended the biogeochemical model to include iSPM in the model formulation (Fig. 2). The model was built with the Fortran-based Framework for Aquatic Biogeochemical Models (FABM) (Bruggeman and Bolding, 2014) to facilitate coupling with the physical model. In this first 140 application, a 1D numerical framework was used, and physical processes in the water column were calculated by GOTM. Simulation resolved the profiles of velocities, temperature, salinity, turbulent mixing, and transport of ecosystem state variables in 20 vertical layers with surface zooming of 1.5 and bottom zooming of 0.1. This approach allows feasible parameterisation, verification, and sensitivity tests to study vertical exchange processes with a low computational effort but hinders the model's capability to represent advection (horizontal transport) and upwelling. However, advection of Atlantic Water is considered to 145 be limited in Hornsund in comparison to other West Spitsbergen fjords, particularly in the inner bays, whereas upwelling of subglacial discharge is most important up to 500 m of distance from the glacier fronts (Pasculli et al., 2020).

The model was implemented at 20 stations located within the newly ice-free areas in Hornsund (Fig. 1b, Tab. 1). The simulations were run from the beginning of 2005 to the end of 2009. Input data from 2005-2009 were averaged, repeated five times, and used as a spin-up to allow the model to reach equilibrium under the applied forcing. Temperature and salinity 150 vertical forcing were used from the 3D hydrodynamic numerical model of Hornsund which represents 9 sources of freshwater input from the Hornsund drainage basin including all components (ablation, precipitation, snow, and rivers) (HMR, Jakacki et al., 2017). Sea-ice thickness and concentration were extracted from the S800 model simulation at the closest grid cells (Albretsen et al., 2017), the same data as used for the HRM model. Sea-ice input was smoothed using a 30-day rolling average, as the 1D setup does not represent advection, and highly variable thickness and concentration affect the performance of the ice 155 algae module. The atmospheric conditions were prescribed from meteorological monitoring in the Polish Polar Station Hornsund, i.e. air temperature (2m above the surface), eastward (*u*) and northward (*v*) wind speed, cloudiness, relative humidity, and pressure. The model was run with a 30-minute time step and the daily average was saved as an output. Two sets of scenarios were performed to evaluate the gains in carbon sequestration potential due to the retreat of marine-terminating

glaciers, and losses due to the iSPM discharge by evaluating plankton primary and secondary production and carbon burial.
 160 The SPM scenario included the iSPM input prescribed to the model according to Eq. (1) and noSPM scenario was a control run without iSPM input.

2.3.1 ECOSMO developments

Two state variables were added to the ECOSMO-E2E-Polar model framework, accounting for iSPM and iSPM sediment pool (sed_{iSPM}) (Fig. 2). The input of iSPM prescribed to the model was calculated based on the inorganic sediment flux (iSF) and
 165 its relationship with air temperature and salinity (Sup. Fig. 1) developed from field data in a form of Eq. (1):

$$iSF = 10^{0.04 \cdot 6accPDD \text{ AT} + 0.174 \cdot (refS - meanS) + 0.815} \quad (1)$$

where $6accPDD \text{ AT}$ is the accumulated daily air temperature for positive degree days for a 6-day window ($^{\circ}\text{C}$), $refS$ is a reference salinity for Atlantic Water (34.9) (Moskalik et al., 2018), and $meanS$ is the mean salinity above the sediment trap. The ordinary least squares (OLS) function (statsmodels library in Python) was used to generate a linear model for iSF estimates.
 170 The root-mean-square deviation (RMSD) was used to measure the differences between the observed iSF and linear model. iSF calculated for each depth layer was prescribed to the model as a daily input ($C_{iSPMinput}$) in $\text{mg} \cdot \text{m}^{-3}$. While some runoff data are available for Hornsund (Van Pelt et al., 2019; Błaszczuk et al., 2019), here it was not feasible to parametrize the iSPM input based on the meltwater discharge due to the structure of the hydrodynamic model (1D in contrast to 3D) and lack of data on sediment loads in glacial plumes. However, in this study, salinity depended on the discharge provided in the 3D hydrodynamic
 175 model that was a source of input data (HMR, Jakacki et al., 2017). Therefore, we used the salinity as a proxy of the inorganic sediment.

The state variables in ECOSMO (full list in Sup. Tab. 3) are solved using prognostic equations in the form of Eq. (2):

$$C_t + (w_d)C_z = (A_v C_z)_z + R_C, \quad (2)$$

with $C_x = \frac{dC}{dx}$, where x represents either time (t) or depth (z). The equation includes vertical turbulent subscale diffusion,
 180 sinking rates and chemical and biological interactions. The vertical turbulent sub-scale diffusion coefficient (A_v) is estimated by the hydrodynamic core of ECOSMO. The sinking rate (w_d) is a constant, non-zero only for detritus, opal, and iSPM. The sinking rate applied in the model that allowed to properly represent the dynamics of iSPM was $0.8 \text{ m} \cdot \text{day}^{-1}$, which is a lower range of sinking rates observed in the field (all parameters are listed in Table 2). Chemical and biological interactions are employed in the interaction term R_C , which is different for each variable (C) based on relevant processes.

185 The rate of change in the iSPM concentration (C_t term) is calculated as Eq. (3):

$$\frac{dC_{iSPM}}{dt} = C_{iSPM} + C_{iSPMinput}, \quad (3)$$

The interaction term R_C is calculated as Eq. (4):

$$R_{iSPM} = [(\lambda_{s2d}C_{sediSPM} - \lambda_{d2s}C_{iSPM})/dz]_{z=bottom}, \quad (4)$$

iSPM enters a new sediment pool with a sedimentation rate (λ_{d2s}) of $3.5 \text{ m}\cdot\text{day}^{-1}$ if bottom stress $< \tau_{crit}$ and a resuspension rate (λ_{s2d}) of 26 day^{-1} if bottom stress $> \tau_{crit}$. Critical bottom shear stress (τ_{crit}) was set to $0.07 \text{ N}\cdot\text{m}^{-2}$, which is in a range reported by Wöfl et al. (2014)Wöfl et al. (2014).

As sed_{iSPM} exchanges occur locally at the bottom and the group is not exposed to mechanical displacement, Eq. (2) is simplified as Eq. (5):

$$\frac{dC_{sediSPM}}{dt} = [R_{sediSPM}]_{z=bottom}, \quad (5)$$

The interaction term R_C is calculated as Eq. (6):

$$R_{sediSPM} = -\lambda_{s2d}C_{sediSPM} + \lambda_{d2s}C_{iSPM}, \quad (6)$$

As the iSPM has an impact on light penetration, the photosynthetically active radiation in the water column has been updated and is calculated as Eq. (7):

$$I(x, y, z, t) = \frac{I_s(x, y)}{2} \exp\left(-k_w z - k_{chl} \int_z^0 \sum_{j=1}^2 Chl_{P_j} \partial z - k_{iSPM} \int_z^0 C_{iSPM} \partial z - k_{DOM} \int_z^0 C_{DOM} \partial z\right), \quad (7)$$

where $I_s(x, y)$ is short wave radiation ($\text{W}\cdot\text{m}^{-2}$) at the surface, x and y identify the horizontal grid points, z is the water depth in m, and k_x are extinction coefficients (Table 2).

In Hornsund, most of the variability of the optical properties in the summers of 2009 and 2010 was attributed to particles of mineral origin (Sagan and Darecki, 2018) therefore the input of organic particles with meltwater was considered negligible here. The attenuation coefficient specific for iSPM measured in another polar fjord in Greenland ($0.13 \text{ m}^2\cdot\text{g}^{-1}$) (Lund-Hansen et al., 2010) was high compared to other published values: $0.07 \text{ m}^2\cdot\text{g}^{-1}$ (Christian and Sheng, 2003), $0.06 \text{ m}^2\cdot\text{g}^{-1}$ (Pfannkuche and Schmidt, 2003), $0.065 \text{ m}^2\cdot\text{g}^{-1}$ (Oliver et al., 2020). Thus, here $0.065 \text{ m}^2\cdot\text{g}^{-1}$ light extinction coefficient (k_{iSPM}) was prescribed to the model, which gave reasonable results in terms of light limitation and is in the range of field measurements. The light limitation also depends on the plankton photosynthesis efficiency parameter (a). Here, it was increased to $0.04 (\text{W}\cdot\text{m}^{-2})^{-1}$, which is within the range reported for Arctic coastal and shelf waters (Van De Poll et al., 2018; Stuart et al., 2000; Strom et al., 2016; Platt et al., 1982) and is in line with previous studies showing that fjord plankton communities are adapted to low light (Simo-Matchim et al., 2016; Holding et al., 2019). The light limitation is calculated as Eq. (8):

$$\alpha(I) = \tanh(a)I(x, y, z, t), \quad (8)$$

In this 1D setup, we do not simulate fish due to their migration, which reduces the uncertainty of the current simulations. Thus, the macrobenthos loss term only consists of excretion ($\varepsilon_{MB}C_{MB}$), and natural mortality ($m_{MB}C_{MB}$) as in Eq. (9):

$$R_{MB_{loss}} = \varepsilon_{MB}C_{MB} + m_{MB}C_{MB}, \quad (9)$$

Similarly, the reaction terms for zooplankton, detritus and DOM were changed accordingly to remove fish grazing (Daewel et al., 2018). Predation mortality from the fish functional group was accounted for by increasing macrobenthos natural mortality (m_{MB}) to 0.03 day^{-1} .

We do not provide nutrient input with meltwater due to the lack of data for parametrisation and to disentangle it from the effect of iSPM discharge; thus, the burial rate in the carbon and nitrogen sediment pool (sedCN, Eq. 10) and Si (Eq. 11) is set to 0 to prevent decreasing nutrient concentrations over the simulation time. For the full description of the equations, the reader is referred to (Daewel and Schrum, 2013). We speculate that the bias introduced by not providing nutrient input is relatively low considering the characteristics of the discharge (see 4.5).

$$R_{sedCN} = \lambda_{d2s}C_D - \lambda_{s2d}C_{sedCN} - \theta(O_2)2\varepsilon_{sedCN}(T)C_{sedCN} - \theta(-O_2)\varepsilon_{sedCNdenit}(T)C_{sedCN} - \delta_{bur}C_{sedCN}, \quad (10)$$

$$R_{sedSi} = \lambda_{d2s}C_{opal} - \lambda_{s2d}C_{sedSi} - \delta_{bur}C_{sedSi}, \quad (11)$$

The carbon burial potential (CB, Eq. 12) was calculated as 70% burial efficiency of the carbon and nitrogen sediment accumulation rate as previously reported for Hornsund (Koziorowska et al., 2018):

$$CB = \eta_{bur}R_{sedCN}, \quad (12)$$

2.4 Model assessment

The satellite data products of suspended particulate matter were not available for the glacial bays and the analysis of the long-term trends and model validation (2005-2009) were not possible here. Thus, we performed the model assessment based on the available field data from 2015-2021. The summertime mean iSPM concentration for the past conditions was reconstructed based on measurements of iSPM concentration and PDD AT, and it showed a high correlation with simulated iSPM concentration parametrized based on the complementary dataset of sediment flux measurements (Sup. Fig. 2, $R^2 = 0.928$, $p = 0.009$). The iSPM concentration at modelled station 2 (HH1) in 2006 and 2009 was also compared with the iSPM field data at monitoring stations M4 (H1_09) and M5 (H1_11) from 2019 (Sup. Fig. 3), which represented environmental conditions (PDD SST, PDD AT, melt season duration, and precipitation in Fig. 3) the closest to the simulation period. Results showed that the model realistically simulated the seasonal pattern and vertical distribution of the iSPM ($\rho > 0.74$, $p < 0.001$ for Spearman's correlation, see Sup. Tab. 4). Even though the iSPM input was parametrized for Hansbukta, which was the only bay with sufficient data, and the iSPM load and discharge can differ between glaciers, the spatial patterns from measurements of iSPM at the surface conducted in all Hornsund in summer 2017 were in line with the simulation results (Sup. Fig. 4). The literature data (Sup. Tab. 5) of concentrations of all the nutrients and functional groups showed that the model performed well when compared to the current knowledge of the West Spitsbergen fjords.

2.5 Data analysis and visualisation

245 The maps and satellite images were generated and processed in ArcGIS Pro 2.8.0. The plots were prepared in Python 3.7 (Van Rossum and Drake, 2009) using Matplotlib 3.1.1 (Caswell et al., 2019), Pandas 1.0.5 (Mckinney, 2010; Reback et al., 2020), and seaborn 0.11.1, and arranged in Inkscape 0.92.4.

The Hamed and Rao modified Mann-Kendall (mMK) test was used to determine whether a trend exists in time series data (SIF, PDD SST, PDD AT, iSPM, precipitation) with a significance level of 0.05 (*) and 0.001 (**) (Python library
250 pymannkendall 1.4.2).

For each modelled station and each scenario, the 5-years (2005-2009) averages of SIC and SIT in May, mean summertime integrated iSPM, and rates of phytoplankton primary production (phyPP), zooplankton secondary production (zooSP), and carbon burial (CB) were calculated. Then, the average values of phyPP, zooSP, and CB rates for all 20 stations were multiplied with the average newly ice-free area between 2006 and 2010 (64.21 km²). The resulting phyPP, zooSP and CB under the SPM
255 scenario were considered as gains in carbon sequestration potential due to the marine-terminating glaciers retreat, whereas the differences between noSPM and SPM scenario were considered as losses due to the iSPM discharge with meltwater.

The influence of iSPM discharge on the ecosystem dynamics was exemplified by presenting biomass of ice algae (IA) and macrobenthos (MB), as well as biomass of phytoplankton (PHY), zooplankton (ZOO), silicate, phosphorus, nitrogen and light limitation index (SIL, PLI, NLI, LLI) integrated for the whole water column at three modelled stations (2, 9, 14) that were
260 comparable due to similar depths (42.45 – 49.55 m), but presented low, intermediate and high level of summertime iSPM input. Also, two years with contrasting sea ice conditions (2008 and 2009) were displayed.

3 Results

3.1 Newly ice-free marine habitats

The areal extent of newly ice-free coastal waters due to the retreat of marine-terminating glaciers in Hornsund increased by
265 ~99.4 km² between the summers of 1976 and 2022 (Fig. 1, 3, around 38% increase in the total area), whereas the volume gained until 2010 was ~3.3 km³. The trends were linear ($y = 2.1406x - 4231.2$; $R^2 = 0.995$ for the area, and $y = 0.097x - 191.38$; $R^2 = 0.984$ for volume, t-test $p < 0.001$) with rates of ~21.4 km²·decade⁻¹ and 1.0 km³·decade⁻¹ (Fig. 3). While advances in glacier fronts due to surge events were observed for some marine-terminating glaciers in Hornsund, these did not influence the overall increasing trends. Along with the glacial retreat, the number of SIF days (fraction of the year with SIC < 15%) increased
270 significantly (~0.1 decade⁻¹, i.e. around 44 days, $p < 0.001$ mMK test). Despite high interannual variability, the central part of Hornsund has become mostly devoid of sea ice since 2006, but there still is seasonal sea ice cover in the newly formed glacial bays (Fig. 6a).

3.2 Melt and SPM discharge potential

The annual sum of daily SST > 0°C (PDD SST), showed no significant trend in outer Hornsund due to strong variability
275 between years ($p > 0.1$ mMK test) (Fig. 3), but it was significantly increasing for summer months (June – August;
46.8°C·decade⁻¹, $p < 0.05$ mMK test). The annual and summertime sum of positive daily air temperatures (PDD AT), as well
as annual precipitation, showed significant increases (60.5°C·decade⁻¹, 31.4°C·decade⁻¹, and 56.0 mm·decade⁻¹, respectively,
 $p < 0.001$ mMK test). Melt season duration increased significantly ($p < 0.001$ mMK test) with a rate of ~9 day·decade⁻¹ (2.5% of
the year). At the beginning of the measurements, the melt season started in June and ended in late September – mid-October,
280 whereas currently it can start as early as February and end mostly in October (Sup. Fig. 5).

The 6-year monitoring dataset of summertime SPM concentration in Hansbukta (Fig. 1c) was not sufficient to show long-term
trends. However, average integrated iSPM levels were correlated with both the annual sum of PDD AT ($y = 0.061x - 19.549$,
 $R^2 = 0.68$, $p < 0.05$ t-test) and the summertime sum of PDD AT (June to August) ($y = 0.221x - 75.047$, $R^2 = 0.78$, $p < 0.05$ t-test).
Even though the correlation was stronger for the summertime PDD AT, the estimates displayed numerous negative values.
285 However, the annual sum of PDD AT allowed a coarse reconstruction of past conditions and revealed significant increases in
iSPM concentration (3.7 g·m⁻³·decade⁻¹ in 1979-2022, $p < 0.001$ mMK test). Importantly, within the modelled time range (2005-
2009, Fig. 3, grey shade), both iSPM estimates gave similar results in 2006 and 2009 (8.6 and 12.0; 8.1 and 9.8 g·m⁻³,
respectively).

3.3 SPM dynamics

The concentration of iSPM varied between seasons with the highest levels in July – October (up to 150 g·m⁻³) and the lowest
290 between November and May (up to 50 g·m⁻³), whereas the highest levels of organic SPM were observed between April and
June (up to 20 g·m⁻³) (Fig. 4a). Sediment flux observed for iSPM ranged between 1 – 6648 g·m⁻²·day⁻¹ while for organic SPM
it was 0.9 – 333 g·m⁻²·day⁻¹ (Fig. 4b). The sinking rate of iSPM ranged between 0.6 – 265 m·day⁻¹ (mean 25.3, median 12.2
m·day⁻¹) (Fig. 4c), while the sinking rate of organic SPM was one order of magnitude lower with a range of 0.3 – 28.9 m·day⁻¹
295 (mean 2.8, median 1.7 m·day⁻¹). The sediment flux of iSPM, which represents temporary dynamics of iSPM input, was
dependent on the accumulated daily air temperature for positive degree days for a 6-day window (6accPDD AT) and mean
salinity in the layer above ($R^2 = 0.662$, $p < 0.001$ t-test, Fig. 4d). Within the range of frequently observed values of 6accPDD
AT (0 – 40°C) and salinity (30 – 35) the estimated inorganic sediment flux could reach up to 1860 g·m⁻²·day⁻¹ (Sup. Fig. 1).
Importantly, the regression model (Eq. 1) performed well for inorganic sediment flux < 2000 g·m⁻²·day⁻¹ (RMSD = 290.1
300 g·m⁻²·day⁻¹), which consisted 95% of the dataset, and mostly underestimated the highest inorganic sediment flux values (RMSD
= 823.3 g·m⁻²·day⁻¹ for all the dataset).

3.4 Spatial patterns of sea-ice, iSPM, plankton production and carbon burial

The mean SIT and SIC in May were the highest in the southern and inner parts of Hornsund (5-year average up to 8 cm and 19.3%, respectively) and the lowest in the northern and outer parts (5-year average of 3 cm and 8.7%, respectively) (Fig. 5a).
305 The mean summertime integrated iSPM concentration was the highest in the inner glacial bay (modelled station 14; 5-year average: $164.4 \text{ g}\cdot\text{m}^{-3}$), where rates of plankton primary and secondary production, and carbon burial were the lowest (5-year average: 11.0, 1.5, and $5.5 \text{ gC}\cdot\text{m}^{-2}\cdot\text{y}^{-1}$, respectively; Fig. 5b,c,d). At other stations, the mean summertime integrated iSPM concentration was in a range between $2.1 - 7.1 \text{ g}\cdot\text{m}^{-3}$ which allowed phyPP to reach rates between $66.3 - 100.7 \text{ gC}\cdot\text{m}^{-2}\cdot\text{y}^{-1}$ (versus $131.3 - 171.2 \text{ gC}\cdot\text{m}^{-2}\cdot\text{y}^{-1}$ under noSPM scenario), whereas rates of zooSP were between $17.7 - 47.2 \text{ gC}\cdot\text{m}^{-2}\cdot\text{y}^{-1}$ (versus $48.7 - 75.7 \text{ gC}\cdot\text{m}^{-2}\cdot\text{y}^{-1}$ under noSPM scenario), and CB rate was in a range of $6.0 - 17.7 \text{ gC}\cdot\text{m}^{-2}\cdot\text{y}^{-1}$ (versus $6.5 - 23.0 \text{ gC}\cdot\text{m}^{-2}\cdot\text{y}^{-1}$ under noSPM). In the simulation period (2005-2009), the newly ice-free areas in Hornsund substantially contributed to phyPP, zooSP, and CB (on average $5.1, 2.0, \text{ and } 0.9 \text{ GgC}\cdot\text{y}^{-1}$, respectively – Fig. 5, green, gains in carbon sequestration potential in SPM scenario). However, the potential was hindered by iSPM input by $5.0, 2.1 \text{ and } 0.1 \text{ GgC}\cdot\text{y}^{-1}$, respectively (Fig. 5, red, loss due to the difference between noSPM and SPM scenario). Thus, without the release of mineral particles, plankton
315 primary and secondary production could have been around two times higher ($10.1, 4.1 \text{ GgC}\cdot\text{y}^{-1}$ under noSPM scenario), whereas carbon burial was less affected by iSPM input ($1.0 \text{ GgC}\cdot\text{y}^{-1}$ under the noSPM scenario, around 16.5% higher than carbon burial under SPM scenario).

3.5 Ecosystem dynamics

The ecosystem dynamics related to the sea ice and iSPM in the newly ice-free areas was presented for three modelled stations
320 with low, intermediate and high influence of iSPM (stations 9, 2, and 14, Fig. 6abc, respectively) in two contrasting years (cold 2008 and warm 2009). The sea ice thickness and concentration (SIT and SIC) were lower in 2008 than in 2009, and in the outer than in the inner glacial bay. Thus, only in 2009 did the ice algae bloom reach up to 0.16 gCm^{-2} biomass in inner Hornsund (9, 14 in Fig. 6a,c) and sea-ice presence (up to 0.5 m) delayed the phytoplankton bloom by around 10 days. Under the low and intermediate influence of iSPM (Fig. 6a,b), the light limitation index was slightly lowered before the main melt season (March to early June) and the significant effect of light limitation due to iSPM input started around late June (up to 24 and 6 gm^{-3} at
325 stations 9, 2 in Fig. 6a,b). Due to the worsened underwater light conditions, the peaks of spring and summer phytoplankton blooms were delayed around 10 – 14 days and the summer peak reached lower biomass ($\sim 0.4 - 0.5 \text{ gC}\cdot\text{m}^{-3}$ under the SPM scenario, and $0.7 \text{ gC}\cdot\text{m}^{-3}$ under noSPM scenario), which further affected zooplankton (peak delayed by ~ 9 days and $0.1 - 0.2 \text{ gC}\cdot\text{m}^{-3}$ less biomass) and macrobenthos ($\sim 10 \text{ gC}\cdot\text{m}^{-2}$ less biomass). At the highest levels of iSPM (up to $500 \text{ g}\cdot\text{m}^{-3}$ at station
330 14, Fig. 6c), strong light limitation started early in March. Thus, phytoplankton, zooplankton, and macrobenthos reached very low biomass ($< 0.2 \text{ gC}\cdot\text{m}^{-3}$, $< 0.05 \text{ gC}\cdot\text{m}^{-3}$, and $< 5 \text{ gC}\cdot\text{m}^{-2}$, respectively). The delays in phytoplankton bloom related to the iSPM led to delays in silicate limitation and increases in the ice algae biomass in spring, particularly at the station with the highest levels of iSPM (up to $0.01 \text{ gC}\cdot\text{m}^{-2}$ difference between SPM and noSPM scenario).

4 Discussion

335 4.1 Newly ice-free marine habitats

We report significant increases in new marine habitat area ($\sim 100 \text{ km}^2$) and volume ($> 3.3 \text{ km}^3$) between 1976–2022 in Hornsund (Fig. 1b, 3, 7a) due to the retreat of marine-terminating glaciers. These results are in line with cryosphere studies in West Spitsbergen fjords (Błaszczuk et al., 2021, 2023; Grabiec et al., 2018; Strzelecki et al., 2020) and in polar regions in general (Kochtitzky et al., 2022; Pfeffer et al., 2014). In the coastal Arctic and Antarctic, glaciers and ice sheets have lost mass due to the increased submarine (basal) melting and iceberg calving (dos Santos et al., 2021; Błaszczuk et al., 2013, 2023), and in Svalbard, a doubling of ice mass loss was predicted by 2100 (Geyman et al., 2022). The retreat of many marine-terminating glaciers has already produced newly ice-free areas, and some of them have receded onto land (Błaszczuk et al., 2013; Jerosch et al., 2019; Kochtitzky et al., 2022). Recently, the rapid loss of numerous glaciers was related to both external forcing such as increases in atmospheric and oceanic temperatures and lack of sea-ice buttressing or internal dynamics such as surges (Błaszczuk et al., 2013, 2023; Strzelecki et al., 2020). Here, we show increasing trends in the length of the melt season ($\sim 9 \text{ day}\cdot\text{decade}^{-1}$) and the sum of positive degree days ($46.79^\circ\text{C}\cdot\text{decade}^{-1}$ for summer PDD SST, $60.54^\circ\text{C}\cdot\text{decade}^{-1}$ and $31.43^\circ\text{C}\cdot\text{decade}^{-1}$ for annual and summer PDD AT, respectively, Fig. 3). While the melting potential is rising, the annual runoff in Svalbard is expected to increase till 2060, then it will likely decrease towards 2100 due to the reduction in glacier storage (Bliss et al., 2014; Van Pelt et al., 2021; Nowak et al., 2021).

350 Furthermore, we report a significant loss in sea ice duration in central Hornsund ($\sim 44 \text{ day}\cdot\text{decade}^{-1}$) (Fig. 3). However, as receding glaciers open new coastal areas, it also increases the potential for winter sea ice formation in the more protected inner bays (Fig. 5a). In contrast to the glaciers where mass loss cannot be stopped nor reversed once induced, sea ice was shown to be more responsive to variations of both ocean and air temperatures (Muckenhuber et al., 2016). Thus, there still can be land-fast ice (sea ice attached to the coastline) covering the inner parts of West Spitsbergen fjords for a limited time during winter and spring. Moreover, the ice bridge in inner Hornsund (Fig. 1b, 7a) is predicted to vanish in the coming decades (2030–2055) (Grabiec et al., 2018; Osika et al., 2022), which will transform Hornsund from a fjord into a strait enabling advection of sea ice from the Barents Sea. However, the loss of the ice bridge could also result in the increased presence of warm Atlantic Water in the area, and therefore, further loss of sea ice. These seemingly contrasting predictions highlight the importance of continuous evaluation of the changing Hornsund environment and its potential as a model area for studies on regime shifts.

360 4.2 SPM dynamics

Based on the coarse reconstruction and modelling results presented in this study, we suggest that the Hornsund bays have already been under the strong influence of dark glacial plumes since the beginning of the simulation period (2005) (Fig. 3, 5ab, 6). In this study, reconstructed iSPM concentration increased after 2013 and further rises are expected ($3.7 \text{ g}\cdot\text{m}^{-3}\cdot\text{decade}^{-1}$ integrated for the water column in summer). We show that air temperature variability, specifically the accumulated daily air temperature above the melting point for 6-day window (6accPDD AT), which considers the delays in meltwater discharge,

modulates the iSPM flux (Fig. 4d, Sup. Fig. 1), similarly as was suggested for a glacial bay further north in Kongsfjorden (D'Angelo et al., 2018). Recent studies also indicated that sediment production and fluxes to the coastal zones in the polar regions have increased due to higher air temperatures (Overeem et al., 2017; Szczuciński et al., 2009). Thus, it is anticipated that even central fjords will receive high input of mineral particles in the future as turbid glacial plumes will spread farther from the source (Fig. 7a) (Castelao et al., 2019; Kanna et al., 2018; Hudson et al., 2014), therefore extending the influence of meltwater discharge onto the shelf and considerably affecting marine systems downstream (Meire et al., 2017, 2015; Milner et al., 2017). The relationship between melting potential and sediment input might differ between catchments, and particularly it could change after glaciers retreat onto land.

The iSPM discharge was the most extensive during summer (Fig. 4), although it could also be observed during autumn and winter, when it is intensified by tidal resuspension, resulting in a relatively high concentration of organic and inorganic suspended particles (Moskalik et al., 2018). In the future, more days with open-water conditions (no sea ice), which can increase wave action and particle removal from the beaches and tidal flats, as well as a longer melt season (Fig. 3, Sup. Fig. 5) could potentially lead to iSPM affecting a substantial part of the productive season, including not only summer and autumn but also spring. Here, we show high variability of iSPM dynamics with sinking rates between $0.6 - 265.9 \text{ m} \cdot \text{day}^{-1}$ and sediment flux between $1.0 - 6647.7 \text{ g} \cdot \text{m}^{-2} \cdot \text{day}^{-1}$ (Fig. 4bc) which should be investigated further in the context of the driving mechanisms such as flocculation (Moskalik et al., 2018).

4.3 Ecosystem dynamics

Observational data and previous modelling studies showed that the continuing retreat of marine-terminating glaciers will negatively affect planktic and benthic communities (Neder et al., 2022; Szeligowska et al., 2022, 2021; Torsvik et al., 2019) especially in enclosed shallow bays such as Brepollen (Fig. 7a). Indeed, we observed decreases in phytoplankton, zooplankton, and macrobenthos biomass, and delays in their peak occurrence close to the glacial fronts (by around 10-14 days as compared to the noSPM scenario, Fig. 5). These decreases were related to the input of particulate matter from land which, even in relatively low concentration in spring, can affect phytoplankton due to light attenuation (Fig. 7b). Under the SPM scenario, plankton primary production rates reached $66.3 - 100.7 \text{ gC} \cdot \text{m}^{-2} \cdot \text{y}^{-1}$ with the mean summertime integrated iSPM concentration of $2.1 - 7.1 \text{ g} \cdot \text{m}^{-3}$, whereas it was around two times higher in the noSPM scenario ($131.3 - 171.2 \text{ gC} \cdot \text{m}^{-2} \cdot \text{y}^{-1}$). Both ranges are comparable with the field measurements in inner and outer Hornsund, and other West Spitsbergen fjords (Hodal et al., 2012; Iversen and Seuthe, 2011; Piwosz et al., 2009; Vonnahme et al., 2021) (Sup. Tab. 5, Sup. Fig. 6). Sea ice algae biomass was extremely low in most years ($<12 \text{ mgC} \cdot \text{m}^{-2}$, except for 2009 – up to $160 \text{ mgC} \cdot \text{m}^{-2}$) due to thin ice ($<50 \text{ cm}$) that disappeared before the main productive season. Ice algae did not seem to be negatively affected by iSPM and, as modeling results suggest, their biomass was slightly higher in the SPM scenario than in the noSPM scenario. Importantly, we suggest that sea ice loss leading to the earlier offset of spring pelagic production might become a compensation mechanism for higher iSPM input in summer (Fig. 7b).

The modelled carbon burial rate was within the reported values (Koziorowska et al., 2018; Kuliński et al., 2014; Zaborska et al., 2018) and it constituted around 10–20% of the primary production, which is also in line with the current observations in polar and sub-polar fjords (Włodarska-Kowalczyk et al., 2019). No field data for the assessment of plankton secondary production rates exists from this region. However, the values simulated here fell between the plankton primary production and carbon burial rates as expected. Plankton secondary production was reduced due to decreased food base ($17.7\text{--}47.2\text{ gC}\cdot\text{m}^{-2}\cdot\text{y}^{-1}$ versus $48.7\text{--}75.7\text{ gC}\cdot\text{m}^{-2}\cdot\text{y}^{-1}$ under the SPM and noSPM scenario, respectively). According to our simulations, carbon burial was the least affected by iSPM ($6.0\text{--}17.7\text{ gC}\cdot\text{m}^{-2}\cdot\text{y}^{-1}$ versus $6.5\text{--}23.0\text{ gC}\cdot\text{m}^{-2}\cdot\text{y}^{-1}$ under SPM and noSPM scenarios, respectively). Since the burial of accumulated material depends on the vertical flux of the organic matter originating from phytoplankton and zooplankton, food intake by benthic fauna, and rates of benthic mineralisation, we hypothesise that the changes in the phytoplankton bloom timing might have shifted the carbon pathway from zooplankton and macrobenthos pool to carbon burial in sediments, and thus carbon burial was still relatively high in the SPM scenario (~16% lower than under noSPM scenario). Only the extremely high levels of iSPM (mean summertime integrated iSPM concentration of $164.4\text{ g}\cdot\text{m}^{-3}$), which can be observed directly inside the turbid plumes, resulted in low biomass of phyto- and zooplankton, and macrobenthos, and in relatively low plankton production rates (11.0 and $1.5\text{ gC}\cdot\text{m}^{-2}\cdot\text{y}^{-1}$ for phyPP and zooSP, respectively), but still considerable burial rates ($5.5\text{ gC}\cdot\text{m}^{-2}\cdot\text{y}^{-1}$). Thus, we speculate that sediment discharge to polar coastal zones might result in less complex food webs, constituted by species better adapted to high iSPM concentrations and sedimentation rates as shown for Antarctic benthos (Clark et al., 2013; Krzemińska and Kukliński, 2018; Sahade et al., 2015). It could reduce the biomass that is utilised in the pelagic and benthic system leading to higher carbon burial in sediments (Fig. 7b).

4.4 Carbon gains and losses

Marine sediments in polar fjords have recently been recognised as efficient organic carbon sinks and incorporated into global carbon burial estimates (Bianchi et al., 2020; Cui et al., 2022; Smith et al., 2015) highlighting its societal importance as a climate regulation ecosystem service (Barnes et al., 2021; Bax et al., 2021). They might become more efficient in the capture-to-long-term carbon sequestration due to high sedimentation rates and their restrictive nature compared to more open coastal environments, particularly with the expansion of the shallow and isolated bays and increased land-ocean connectivity (Fig. 7b) (Smith et al., 2015). Here, we show that newly ice-free areas in Hornsund (~64 km² between 2006–2010) markedly contributed to plankton primary ($5.1\text{ GgC}\cdot\text{y}^{-1}$) and secondary production ($2.0\text{ GgC}\cdot\text{y}^{-1}$), and carbon burial ($0.9\text{ GgC}\cdot\text{y}^{-1}$) (greens in Fig. 6, carbon gains under SPM scenario). This carbon burial rate constitutes only a small fraction of the estimates for seafloor globally ($2.9\cdot 10^4\text{--}1.6\cdot 10^5\text{ GgC}\cdot\text{y}^{-1}$; Bauer et al., 2013; Cai, 2011; Hedges and Keil, 1995). However, emerging marine habitats could gain more relevance considering that organic carbon burial efficiency in fjords is two times higher than the global ocean average (Smith et al., 2015) and recognising the scale of marine ice loss in polar regions. Due to the anticipated negative effects of glacier ice loss (Hunter, 2022), here we show that part of the potential gains in carbon sequestration related to the newly ice-free areas turns into losses for plankton primary ($-5.0\text{ GgC}\cdot\text{y}^{-1}$) and secondary production ($-2.1\text{ GgC}\cdot\text{y}^{-1}$), and burial (-0.1

430 GgC·y⁻¹) under the SPM scenario (Fig. 6, red). Without the delivery of mineral particles from land, plankton primary and secondary production could have been around two times higher (10.1 and 4.1 GgC·y⁻¹ under noSPM scenario, respectively), whereas carbon burial was less affected by iSPM input (1.0 GgC·y⁻¹ under noSPM scenario). Importantly, the carbon burial efficiency is highly variable and differs between fjords (Koziorowska et al., 2018), thus limiting generalisations.

4.5 Current limitations and future perspectives

435 While the coupled physical-biogeochemical model with newly implemented iSPM input performed well according to our assessment, the field data for model parametrisation and validation were not available for the simulated period (2005–2009), whereas remotely-sensed products for iSPM concentration did not cover the inner fjords and were frequently limited by clouds. Despite that, the reconstructions of previous conditions and assessment based on the two complementary datasets collected in recent years (2015–2021, SPM and sediment flux) suggest that the simulated spatial and temporal dynamics of both inorganic
440 and organic SPM was rather realistic and in line with the current knowledge of the West Spitsbergen marine ecosystem. While it should be considered that this reconstruction was based on a few years of measurements, which might limit its robustness, particularly towards the beginning of AT measurements, the correlation with annual PDD AT seems to yield reasonable estimates. A recent multi-year study (2010-2016) in another West Spitsbergen fjord (Kongsfjorden) also indicated the relationship between particle fluxes and air temperature above the melting point (D'Angelo et al., 2018). Notably, the satellite
445 data products calibrated for the glacial bays should become available (Klein et al., 2021; Walch et al., 2022) to verify the long-term trends in the iSPM discharge revealed in this study.

In this study, we used the meteorological forcing from observations performed at the Polish Polar Station located in the outer part of Hornsund for all the modelled stations, since there is no long-term weather monitoring in the inner fjord. A previous study showed that in summer, the air temperature in the inner fjord was lower by 0.6-1°C than values reported for Polish Polar
450 Station, and the highest difference was observed during winter (around 2°C) (Arażny et al., 2018). While the proper atmospheric representation is crucial and, in general, the spatial variations could affect the results, the differences in daily temperatures (AT), and precipitation were relatively low between the inner and outer fjord according to atmospheric fields derived from ERA-interim reanalysis (Dee et al., 2011) (Sup. Fig. 7). It could be related to the fact that Hornsund is a small fjord with an opening mostly influenced by Sørkapp Current transporting Arctic Water from the Barents Sea. The polar front
455 that exists there reduces the advection of warm Atlantic Water into Hornsund. Thus, the entire area retains the arctic properties unlike other West Spitsbergen fjords (Promińska et al., 2017; Cisek et al., 2017).

So far, only a few numerical models have been implemented to study the dynamics of SPM input from land in polar and subpolar regions. 3D models have indicated the areas with long residence time and high accumulation rates of iSPM (Neder et al., 2022) and considered a light limitation that led to the shallowing of the photic zone within the dark plumes (Le Fouest et al., 2010; Marín et al., 2013; Møller et al., 2023). Moreover, 2D models have been developed to simulate the sedimentation induced by ice-rafted debris (Mugford and Dowdeswell, 2010), and by glacial meltwater plumes emerging from marine-terminating glaciers (Dowdeswell et al., 2015; Mugford and Dowdeswell, 2011). However, due to the various data, processes

represented, and numerical models available for the respective regions, they differ in the parametrisation and approach, both between each other and our study. To the best of our knowledge, this is one of the first attempts to implement the influence of iSPM in the coupled physical-biogeochemical model in polar coastal zones. While this 1D approach does not represent upwelling nor spatial fluctuations in the glacial plumes, e.g. implemented in Hansbukta in 2D (De Andrés et al., 2018, 2021), or flocculation of the particles (Dowdeswell et al., 2015; Mugford and Dowdeswell, 2011), it is a first step to address the technical challenges related to the coupling between the sympagic, pelagic and benthic systems and their response to glacial discharge and retreat.

Even though Hornsund is amongst the most studied Svalbard fjords, our study was limited to 5 years period due to the lack of long-term input data for temperature and salinity (Jakacki et al., 2017; Torsvik et al., 2019) as most of the hydrodynamic models do not simulate coastal zones with sufficient horizontal resolution and they do not consider changes in the extent of glacial bays. It should also be considered that sea ice concentration and thickness were extracted from the closest data points available, and thus sea ice conditions might have been different in the glacial bays. However, smoothing the data for more stable model runs could have resulted in more accurate forcing. Also, the advection of Atlantic Water is not represented in this 1D setup, but due to the strong boundary in the form of polar front and sills, most of the primary and secondary production in glacial bays of Hornsund is assumed to be local, contrary to other West Spitsbergen sill-free fjords experiencing high advection of plankton (Basedow et al., 2004; Gluchowska et al., 2016).

Here, we disentangled the effects of iSPM input from other factors such as organic matter and nutrient delivery with meltwater. The influence of terrestrial organic matter on light attenuation was assumed negligible in Hornsund for the time of simulation (Sagan and Darecki, 2018). However, the release of large amounts of petrogenic organic carbon that has been isolated under the ice for millennia is recently emerging as an important input for carbon burial in fjords (Fig. 7b) but also a source for microbial recycling leading to greenhouse gas emissions (Ruben et al., 2023). These pathways should be better constrained for the future model development. Moreover, several modelling and field studies in arctic coastal waters have shown that the upwelling effect of submarine plumes and nutrient fluxes with meltwater supports primary production in the glacial bays and on the shelf (Castelao et al., 2019; Luo et al., 2016; McGovern et al., 2020; Oliver et al., 2020). Yet, the net effect depends on the lithology, subglacial discharge rate and depth of the glacier grounding line, as well as the seasonal dynamics of coastal currents, winds, and eddy activity, and it was not possible to represent it properly in this study. Studies in Greenland fjords indicate that macronutrients were primarily supplied to the surface waters by mixing and not transported by glacial meltwater from land as it was shown to have a relatively low nutrient load (Hopwood et al., 2020). However, Svalbard fjords are relatively shallow, and thus the upwelling pump might not be as efficient as for Greenland fjords or the shallower, nutrient-deficient waters might be transported (Hopwood et al., 2018). Furthermore, while macronutrient concentrations can be higher in the arctic rivers, most of the discharge in Hornsund comes from marine-terminating glaciers (Błaszczuk et al., 2019). Also, rivers were shown to deliver nutrients mostly in August (McGovern et al., 2020), when phytoplankton is already limited due to the light attenuation by iSPM. Even though nutrient input was not provided, setting the nutrient burial rate to 0 allowed keeping the nutrients in the system that would otherwise be excluded, and it could compensate to some degree for the lack of nutrient

input with meltwater. Thus, the overall bias introduced by not providing nutrient input in our simulations might be relatively low.

500 The ecosystem dynamics is a result of the combined interaction of, inter alia, dynamic coastline, hydrographic and sea-ice conditions, nutrients and sediment discharge, and thus this interdisciplinary work adds to the current understanding of the complex influence of glaciers on marine productivity and carbon fluxes (Hopwood et al., 2020). The presented numerical framework allows to disentangle the effects of various processes, and therefore facilitates efficient hypothesis testing. Despite inherent weaknesses, it provides reliable results contrastable with the field measurements. The limitations of this study could be readily addressed by further development and implementation of high-resolution general circulation models in polar regions
505 (Szeligowska et al., in review) and coupling with biogeochemical modules such as those presented here. Thus, skilful 3D fine-scale ecosystem models could arise from such work in the future.

5 Conclusions

In this study, we used Hornsund as a model high-latitude fjord particularly sensitive to a changing climate. We presented the accumulated effects of interactions between the atmosphere, ocean, cryosphere, and the dynamic coastline, and how these
510 affect the carbon sequestration potential. By combining the results of numerical modelling, remote sensing, and in situ observations, we provided a broad view of the periglacial environment and a framework for future simulations of ecosystem dynamics affected by terrigenous matter input with meltwater. Relatively well-studied areas adjacent to rapidly retreating marine-terminating glaciers in Hornsund are representative of similar coastal environments and, therefore, shed light on the formation and development of new marine habitats not only on a local but also on a regional scale. Thus, the findings are
515 potentially important for predictions in other regions such as Greenland, Patagonia, Alaska, and the Antarctic Peninsula, which experience temperatures close to, or above the melting point and hence are exposed to similar warming effects. Here, we show that despite the negative influence of iSPM input, the loss of marine ice in polar regions can be expected to ultimately lead to higher net productivity and the emergence of carbon sinks due to the formation of newly ice-free areas. Thus, glacial retreat and terrigenous matter input should be implemented in current ocean models applied to such coastal systems to resolve carbon
520 fluxes more accurately. However, the intertwined complexity of changes in high-Arctic coastal zones complicates the estimation of net effects on carbon burial in sediments. Considerable uncertainties remain, in particular related to the petrogenic organic carbon release. Here, we also highlight the importance of maintaining long-term observations and implementing FAIR principles (findability, accessibility, interoperability, reusability) in data infrastructures to improve our understanding of the evolution of deglaciating coasts and subsequent influences on the marine ecosystem, which is one of the research priorities in
525 the context of climate change impacts on polar regions.

6 Data availability

The satellite images are available at <https://glovis.usgs.gov/app>. Meteorological data from Hornsund were downloaded from <https://doi.pangaea.de/10.1594/PANGAEA.909042> and <https://doi.org/10.5194/essd-12-805-2020>. Datasets for suspended particulate matter, sediment flux, and salinity were downloaded from <https://dataportal.igf.edu.pl/group/longhorn>. Arctic Sea and Ice Surface Temperature datasets were deposited at <https://doi.org/10.6084/m9.figshare.24142965> and results of numerical simulations were stored at <https://doi.org/10.6084/m9.figshare.24143013> and <https://doi.org/10.6084/m9.figshare.24142992>.

7 Authors contribution

Contributed to conception and design: MS, DB, BM

Contributed to acquisition of data: MS, AP, DB, MM

535 Contributed to analysis and interpretation of data: MS, DB, MM, BM

Drafted the article: MS

Revised the article: MS, DB, AP, BM, MM, ET, KBS

Approved the submitted version for publication: MS, DB, AP, BM, MM, ET, KBS

8 Competing interests

540 The authors declare that they have no conflict of interest.

9 Acknowledgements

MS, ET, KBS were funded by Polish National Science Centre project (NCN, CoastDark 2018/29/B/NZ8/02463). MS, MM, ET were supported by project financed within the GRIEG competition funded by the Norwegian Financial Mechanism 2014-2021 (No. of agreement: UMO-2019/34/H/ST10/00504). MS was additionally funded by DAAD short-term research grant 545 2020 (57507441) and NAWA Bekker programme (BPN/BEK/2021/1/00258). DB was supported by Changing Arctic Ocean project MiMeMo (NE/R012679/1) jointly funded by the UKRI Natural Environment Research Council (NERC) and the German Federal Ministry of Education and Research (BMBF/03F0801A). Data was collected in the LONGHORN - oceanographical monitoring realized in Polish Polar Station Hornsund.

10 References

- 550 Albretsen, J., Hattermann, T., and Sundfjord, A.: Ocean and sea ice circulation model results from Svalbard area (ROMS [v3.5]), Norwegian Polar Institute, 2017.
- Araźny, A., Przybylak, R., Wyszynski, P., Wawrzyniak, T., Nawrot, A. and Budzik, T.: Spatial variations in air temperature and humidity over Hornsund fjord (Spitsbergen) from 1 July 2014 to 30 June 2015, *Geografiska Annaler: Series A, Physical Geography*, 100, 1, pp.27-43, <https://doi.org/10.1080/04353676.2017.13688322018>.
- 555 De Andrés, E., Otero, J., Navarro, F., Promińska, A., Lapazaran, J., and Walczowski, W.: A two-dimensional glacier-fjord coupled model applied to estimate submarine melt rates and front position changes of Hansbreen, Svalbard, *Journal of Glaciology*, 64, 745–758, <https://doi.org/10.1017/jog.2018.61>, 2018.
- De Andrés, E., Otero, J., Navarro, F. J., and Walczowski, W.: Glacier-plume or glacier-fjord circulation models? A 2-D comparison for Hansbreen-Hansbukta system, Svalbard, *Journal of Glaciology*, 67, 797–810, <https://doi.org/10.1017/jog.2021.27>, 2021.
- 560 Ardyna, M. and Arrigo, K. R.: Phytoplankton dynamics in a changing Arctic Ocean, <https://doi.org/10.1038/s41558-020-0905-y>, 1 October 2020.
- Arntsen, M., Sundfjord, A., Skogseth, R., Błaszczuk, M., and Promińska, A.: Inflow of Warm Water to the Inner Hornsund Fjord, Svalbard: Exchange Mechanisms and Influence on Local Sea Ice Cover and Glacier Front Melting, *J Geophys Res*
- 565 *Oceans*, 124, 1915–1931, <https://doi.org/10.1029/2018JC014315>, 2019.
- Arrigo, K. R., van Dijken, G., and Pabi, S.: Impact of a shrinking Arctic ice cover on marine primary production, *Geophys Res Lett*, 35, <https://doi.org/10.1029/2008GL035028>, 2008.
- Barnes, D. K. A.: Polar zoobenthos blue carbon storage increases with sea ice losses, because across-shelf growth gains from longer algal blooms outweigh ice scour mortality in the shallows, *Glob Chang Biol*, 23, 5083–5091, <https://doi.org/10.1111/gcb.13772>, 2017.
- 570 Barnes, D. K. A., Sands, C. J., Paulsen, M. L., Moreno, B., Moreau, C., Held, C., Downey, R., Bax, N., Stark, J., and Zwerschke, N.: Societal importance of Antarctic negative feedbacks on climate change: blue carbon gains from sea ice, ice shelf and glacier losses, <https://doi.org/10.1007/s00114-021-01748-8>, 1 October 2021.
- Basedow, S. L., Eiane, K., Tverberg, V., and Spindler, M.: Advection of zooplankton in an Arctic fjord (Kongsfjorden, Svalbard), *Estuar Coast Shelf Sci*, 60, 113–124, <https://doi.org/10.1016/j.ecss.2003.12.004>, 2004.
- 575 Bauer, J. E., Cai, W. J., Raymond, P. A., Bianchi, T. S., Hopkinson, C. S., and Regnier, P. A. G.: The changing carbon cycle of the coastal ocean, <https://doi.org/10.1038/nature12857>, 5 December 2013.
- Bax, N., Sands, C. J., Gogarty, B., Downey, R. V., Moreau, C. V. E., Moreno, B., Held, C., Paulsen, M. L., McGee, J., Haward, M., and Barnes, D. K. A.: Perspective: Increasing blue carbon around Antarctica is an ecosystem service of considerable
- 580 societal and economic value worth protecting, *Glob Chang Biol*, 27, 5–12, <https://doi.org/10.1111/gcb.15392>, 2021.

- Benkert, D., Daewel, U., Heath, M., and Schrum, C.: On the Role of Biogeochemical Coupling Between Sympagic and Pelagic Ecosystem Compartments for Primary and Secondary Production in the Barents Sea, *Front Environ Sci*, 8, 548013, <https://doi.org/10.3389/fenvs.2020.548013>, 2020.
- 585 Berner, R. A.: Burial of organic carbon and pyrite sulfur in the modern ocean: Its geochemical and environmental significance, *Am J Sci*, 282, 451–473, <https://doi.org/10.2475/ajs.282.4.451>, 1982.
- Bianchi, T. S., Arndt, S., Austin, W. E. N., Benn, D. I., Bertrand, S., Cui, X., Faust, J. C., Kozirowska-Makuch, K., Moy, C. M., Savage, C., Smeaton, C., Smith, R. W., and Syvitski, J.: Fjords as Aquatic Critical Zones (ACZs), <https://doi.org/10.1016/j.earscirev.2020.103145>, 1 April 2020.
- 590 Blain, C. O., Hansen, S. C., and Shears, N. T.: Coastal darkening substantially limits the contribution of kelp to coastal carbon cycles, *Glob Chang Biol*, 27, 5547–5563, <https://doi.org/10.1111/gcb.15837>, 2021.
- Bliss, A., Hock, R., & Radić, V.: Global response of glacier runoff to twenty-first century climate change. *Journal of Geophysical Research: Earth Surface*, 119, 4, 717–730, <https://doi.org/10.1002/2013JF002931>, 2014.
- Błaszczuk, M., Jania, J. A., and Kolondra, L.: Fluctuations of tidewater glaciers in Hornsund Fjord (Southern Svalbard) since the beginning of the 20th century, *Pol Polar Res*, 34, 327–352, <https://doi.org/10.2478/popore-2013-0024>, 2013.
- 595 Błaszczuk, M., Ignatiuk, D., Uszczyk, A., Cielecka-Nowak, K., Grabiec, M., Jania, J. A., Moskalik, M., and Walczowski, W.: Freshwater input to the arctic fjord hornsund (Svalbard), *Polar Res*, 38, <https://doi.org/10.33265/polar.v38.3506>, 2019.
- Błaszczuk, M., Jania, J. A., Ciepły, M., Grabiec, M., Ignatiuk, D., Kolondra, L., Kruss, A., Luks, B., Moskalik, M., Pastusiak, T., Strzelewicz, A., Walczowski, W., and Wawrzyniak, T.: Factors Controlling Terminus Position of Hansbreen, a Tidewater Glacier in Svalbard, *J Geophys Res Earth Surf*, 126, e2020JF005763, <https://doi.org/10.1029/2020JF005763>, 2021.
- 600 Błaszczuk, M., Moskalik, M., Grabiec, M., Jania, J., Walczowski, W., Wawrzyniak, T., Strzelewicz, A., Malnes, E., Lauknes, T. R., and Pfeffer, W. T.: The Response of Tidewater Glacier Termini Positions in Hornsund (Svalbard) to Climate Forcing, 1992–2020, *J Geophys Res Earth Surf*, 128, e2022JF006911, <https://doi.org/10.1029/2022JF006911>, 2023.
- Bruggeman, J. and Bolding, K.: A general framework for aquatic biogeochemical models, *Environmental Modelling and Software*, 61, 249–265, <https://doi.org/10.1016/j.envsoft.2014.04.002>, 2014.
- 605 Burchard, H., Bolding, K., and Villarreal, M. R.: GOTM—A general ocean turbulence model. Theory, applications and test cases., 103 pp., 1999.
- Cai, W.-J.: Estuarine and Coastal Ocean Carbon Paradox: CO₂ Sinks or Sites of Terrestrial Carbon Incineration?, *Ann Rev Mar Sci*, 3, 123–145, <https://doi.org/10.1146/annurev-marine-120709-142723>, 2011.
- Castelao, R. M., Luo, H., Oliver, H., Rennermalm, A. K., Tedesco, M., Bracco, A., Yager, P. L., Mote, T. L., and Medeiros, P. M.: Controls on the Transport of Meltwater From the Southern Greenland Ice Sheet in the Labrador Sea, *J Geophys Res Oceans*, 124, 3551–3560, <https://doi.org/10.1029/2019JC015159>, 2019.
- 610 Caswell, T. A., Droettboom, M., Hunter, J., Lee, A., Firing, E., Stansby, D., Klymak, J., Andrade, E. S. de, Nielsen, J. H., Varoquaux, N., Hoffmann, T., Root, B., Elson, P., May, R., Dale, D., Lee, J.-J., Seppänen, J. K., McDougall, D., Straw, A.,

- Hobson, P., Gohlke, C., Yu, T. S., Ma, E., Vincent, A. F., Silvester, S., Moad, C., Katins, J., Kniazev, N., Ariza, F., and Ernest, E.: *matplotlib/matplotlib: REL: v3.1.1*, <https://doi.org/10.5281/ZENODO.3264781>, 2019.
- Christian, D. and Sheng, Y. P.: Relative influence of various water quality parameters on light attenuation in Indian River Lagoon, *Estuar Coast Shelf Sci*, 57, 961–971, [https://doi.org/10.1016/S0272-7714\(03\)00002-7](https://doi.org/10.1016/S0272-7714(03)00002-7), 2003.
- Cisek, M., Makuch, P. and Petelski, T.: Comparison of meteorological conditions in Svalbard fjords: Hornsund and Kongsfjorden. *Oceanologia*, 59, 4, pp.413-421, <https://doi.org/10.1016/j.oceano.2017.06.004>, 2017.
- Clark, G.F., Stark, J.S., Johnston, E.L., Runcie, J.W., Goldsworthy, P.M., Raymond, B. and Riddle, M.J.: Light-driven tipping points in polar ecosystems. *Global Change Biology*, 19, 12, pp.3749-3761, <https://doi.org/10.1111/gcb.12337>, 2013.
- Cui, X., Mucci, A., Bianchi, T. S., He, D., Vaughn, D., Williams, E. K., Wang, C., Smeaton, C., Koziarowska-Makuch, K., Faust, J. C., Plante, A. F., and Rosenheim, B. E.: Global fjords as transitory reservoirs of labile organic carbon modulated by organo-mineral interactions, *Sci Adv*, 8, <https://doi.org/10.1126/sciadv.add0610>, 2022.
- Daewel, U. and Schrum, C.: Simulating long-term dynamics of the coupled North Sea and Baltic Sea ecosystem with ECOSMO II: Model description and validation, *Journal of Marine Systems*, 119–120, 30–49, <https://doi.org/10.1016/j.jmarsys.2013.03.008>, 2013.
- Daewel, U., Schrum, C., and Macdonald, J.: Towards End-2-End modelling in a consistent NPZD-F modelling framework (ECOSMOE2E_vs1.0): Application to the North Sea and Baltic Sea, *Geoscientific Model Development Discussions*, 1–40, <https://doi.org/10.5194/gmd-2018-239>, 2018.
- D’Angelo, A., Giglio, F., Misericocchi, S., Sanchez-Vidal, A., Aliani, S., Tesi, T., Viola, A., Mazzola, M., and Langone, L.: Multi-year particle fluxes in Kongsfjorden, Svalbard, *Biogeosciences*, 15, 5343–5363, <https://doi.org/10.5194/bg-15-5343-2018>, 2018.
- Dee, D.P., Uppala, S.M., Simmons, A.J., Berrisford, P., Poli, P., Kobayashi, S., Andrae, U., Balmaseda, M.A., Balsamo, G., Bauer, D.P. and Bechtold, P.: The ERA-Interim reanalysis: Configuration and performance of the data assimilation system. *Quarterly Journal of the royal meteorological society*, 137, 656, pp.553-597, <https://doi.org/10.1002/qj.828>, 2011.
- Deregibus, D., Quartino, M. L., Campana, G. L., Momo, F. R., Wiencke, C., and Zacher, K.: Photosynthetic light requirements and vertical distribution of macroalgae in newly ice-free areas in Potter Cove, South Shetland Islands, Antarctica, *Polar Biol*, 39, 153–166, <https://doi.org/10.1007/s00300-015-1679-y>, 2016.
- Dowdeswell, J. A., Hogan, K. A., Arnold, N. S., Mugford, R. I., Wells, M., Hirst, J. P. P., and Decalf, C.: Sediment-rich meltwater plumes and ice-proximal fans at the margins of modern and ancient tidewater glaciers: Observations and modelling, *Sedimentology*, 62, 1665–1692, <https://doi.org/10.1111/sed.12198>, 2015.
- Duarte, C. M., Middelburg, J. J., and Caraco, N.: Major role of marine vegetation on the oceanic carbon cycle, *Biogeosciences*, 2, 1–8, <https://doi.org/10.5194/bg-2-1-2005>, 2005.
- Fadeev, E., Rogge, A., Ramondenc, S., Nöthig, E. M., Wekerle, C., Bienhold, C., Salter, I., Waite, A. M., Hehemann, L., Boetius, A., and Iversen, M. H.: Sea ice presence is linked to higher carbon export and vertical microbial connectivity in the Eurasian Arctic Ocean, *Commun Biol*, 4, 1–13, <https://doi.org/10.1038/s42003-021-02776-w>, 2021.

- Ficetola, G. F., Marta, S., Guerrieri, A., Gobbi, M., Ambrosini, R., Fontaneto, D., Zerboni, A., Poulenard, J., Caccianiga, M., and Thuiller, W.: Dynamics of Ecological Communities Following Current Retreat of Glaciers, *Annu Rev Ecol Evol Syst*, 52, 650 <https://doi.org/10.1146/annurev-ecolsys-010521-040017>, 2021.
- Le Fouest, V., Zakardjian, B., and Saucier, F. J.: Plankton ecosystem response to freshwater-associated bulk turbidity in the subarctic Gulf of St. Lawrence (Canada): A modelling study, *Journal of Marine Systems*, 81, 75–85, <https://doi.org/10.1016/j.jmarsys.2009.12.003>, 2010.
- Geyman, E. C., J. J. van Pelt, W., Maloof, A. C., Aas, H. F., and Kohler, J.: Historical glacier change on Svalbard predicts doubling of mass loss by 2100, *Nature*, 601, 374–379, <https://doi.org/10.1038/s41586-021-04314-4>, 2022.
- Gluchowska, M., Kwasniewski, S., Prominska, A., Olszewska, A., Goszczko, I., Falk-Petersen, S., Hop, H., and Weslawski, J. M.: Zooplankton in Svalbard fjords on the Atlantic–Arctic boundary, *Polar Biol*, 39, 1785–1802, <https://doi.org/10.1007/s00300-016-1991-1>, 2016.
- Grabiec, M., Ignatiuk, D., Jania, J. A., Moskalik, M., Głowacki, P., Błaszczuk, M., Budzik, T., and Walczowski, W.: Coast 660 formation in an Arctic area due to glacier surge and retreat: The Hornbreen-Hambergreen case from Spistbergen, *Earth Surf Process Landf*, 43, 387–400, <https://doi.org/10.1002/esp.4251>, 2018.
- Hedges, J. I. and Keil, R. G.: Sedimentary organic matter preservation: an assessment and speculative synthesis, [https://doi.org/10.1016/0304-4203\(95\)00008-F](https://doi.org/10.1016/0304-4203(95)00008-F), 1 April 1995.
- Hock, R.: Glacier melt: a review of processes and their modelling, *Progress in Physical Geography: Earth and Environment*, 665 29, 362–391, <https://doi.org/10.1191/0309133305pp453ra>, 2005.
- Hodal, H., Falk-Petersen, S., Hop, H., Kristiansen, S., and Reigstad, M.: Spring bloom dynamics in Kongsfjorden, Svalbard: Nutrients, phytoplankton, protozoans and primary production, *Polar Biol*, 35, 191–203, <https://doi.org/10.1007/s00300-011-1053-7>, 2012.
- Holding, J. M., Markager, S., Juul-Pedersen, T., Paulsen, M. L., Møller, E. F., Meire, L., and Sejr, M. K.: Seasonal and spatial 670 patterns of primary production in a high-latitude fjord affected by Greenland Ice Sheet run-off, *Biogeosciences*, 16, 3777–3792, <https://doi.org/10.5194/bg-16-3777-2019>, 2019.
- Holt, J., Schrum, C., Cannaby, H., Daewel, U., Allen, I., Artioli, Y., Bopp, L., Butenschon, M., Fach, B. A., Harle, J., Pushpadas, D., Salihoglu, B., and Wakelin, S.: Potential impacts of climate change on the primary production of regional seas: A comparative analysis of five European seas, *Prog Oceanogr*, 140, 91–115, <https://doi.org/10.1016/j.pocean.2015.11.004>, 675 2016.
- Hopwood, M. J., Carroll, D., Browning, T. J., Meire, L., Mortensen, J., Krisch, S., and Achterberg, E. P.: Non-linear response of summertime marine productivity to increased meltwater discharge around Greenland, *Nat Commun*, 9, 1–9, <https://doi.org/10.1038/s41467-018-05488-8>, 2018.
- Hopwood, M. J., Carroll, D., Dunse, T., Hodson, A., Holding, J. M., Iriarte, J. L., Ribeiro, S., Achterberg, E. P., Cantoni, C., 680 Carlson, D. F., Chierici, M., Clarke, J. S., Cozzi, S., Fransson, A., Juul-Pedersen, T., Winding, M. H. S., and Meire, L.: Review

- article: How does glacier discharge affect marine biogeochemistry and primary production in the Arctic?, <https://doi.org/10.5194/tc-14-1347-2020>, 24 April 2020.
- Howard, J., Hoyt, S., Isensee, K., Telszewski, M., and Pidgeon, E.: Coastal blue carbon: methods for assessing carbon stocks and emissions factors in mangroves, tidal salt marshes, and seagrasses, 2014.
- 685 Hudson, B., Overeem, I., Mcgrath, D., Syvitski, J. P. M., Mikkelsen, A., and Hasholt, B.: MODIS observed increase in duration and spatial extent of sediment plumes in Greenland fjords, *Cryosphere*, 8, 1161–1176, <https://doi.org/10.5194/tc-8-1161-2014>, 2014.
- Hunter, W. R.: Can carbon storage in West Antarctic fjords have an impact on climate change, following glacier retreat?, *Glob Chang Biol*, 28, 1703–1704, <https://doi.org/10.1111/gcb.16047>, 2022.
- 690 Iversen, K. R. and Seuthe, L.: Seasonal microbial processes in a high-latitude fjord (Kongsfjorden, Svalbard): I. Heterotrophic bacteria, picoplankton and nanoflagellates, *Polar Biol*, 34, 731–749, <https://doi.org/10.1007/s00300-010-0929-2>, 2011.
- Jakacki, J., Przyborska, A., Kosecki, S., Sundfjord, A., and Albrechtsen, J.: Modelling of the Svalbard fjord Hornsund, *Oceanologia*, 59, 473–495, <https://doi.org/10.1016/j.oceano.2017.04.004>, 2017.
- Jerosch, K., Scharf, F. K., Deregibus, D., Campana, G. L., Zacher, K., Pehlke, H., Falk, U., Christian Hass, H., Quartino, M.
695 L., and Abele, D.: Ensemble modeling of Antarctic macroalgal habitats exposed to glacial melt in a polar fjord, *Front Ecol Evol*, 7, 207, <https://doi.org/10.3389/fevo.2019.00207>, 2019.
- Kanna, N., Sugiyama, S., Ohashi, Y., Sakakibara, D., Fukamachi, Y., and Nomura, D.: Upwelling of Macronutrients and Dissolved Inorganic Carbon by a Subglacial Freshwater Driven Plume in Bowdoin Fjord, Northwestern Greenland, *J Geophys Res Biogeosci*, 123, 1666–1682, <https://doi.org/10.1029/2017JG004248>, 2018.
- 700 Klein, K. P., Lantuit, H., Heim, B., Doxaran, D., Juhls, B., Nitze, I., Walch, D., Poste, A., and Søreide, J. E.: The Arctic Nearshore Turbidity Algorithm (ANTA) - A multi sensor turbidity algorithm for Arctic nearshore environments, *Science of Remote Sensing*, 4, 100036, <https://doi.org/10.1016/J.SRS.2021.100036>, 2021.
- Kochtitzky, W., Copland, L., Van Wychen, W., Hugonnet, R., Hock, R., Dowdeswell, J. A., Benham, T., Strozzi, T., Glazovsky, A., Lavrentiev, I., Rounce, D. R., Millan, R., Cook, A., Dalton, A., Jiskoot, H., Cooley, J., Jania, J., and Navarro,
705 F.: The unquantified mass loss of Northern Hemisphere marine-terminating glaciers from 2000–2020, *Nat Commun*, 13, 1–10, <https://doi.org/10.1038/s41467-022-33231-x>, 2022.
- Koziorowska, K., Kuliński, K., and Pempkowiak, J.: Comparison of the burial rate estimation methods of organic and inorganic carbon and quantification of carbon burial in two high Arctic fjords, *Oceanologia*, 60, 405–418, <https://doi.org/10.1016/j.oceano.2018.02.005>, 2018.
- 710 Krzeminska, M. and Kuklinski, P.: Biodiversity patterns of rock encrusting fauna from the shallow sublittoral of the Admiralty Bay. *Marine environmental research*, 139, pp.169-181, <https://doi.org/10.1016/j.marenvres.2018.03.016>, 2018.
- Kuliński, K., Kedra, M., Legeżyńska, J., Gluchowska, M., and Zaborska, A.: Particulate organic matter sinks and sources in high Arctic fjord, *Journal of Marine Systems*, 139, 27–37, <https://doi.org/10.1016/j.jmarsys.2014.04.018>, 2014.

- Lalande, C., Nöthig, E., and Fortier, L.: Algal Export in the Arctic Ocean in Times of Global Warming, *Geophys Res Lett*, 46, 5959–5967, <https://doi.org/10.1029/2019GL083167>, 2019.
- Luckman, A., Benn, D.I., Cottier, F., Bevan, S., Nilsen, F. and Inall, M.: Calving rates at tidewater glaciers vary strongly with ocean temperature. *Nature communications*, 6, 1, p.8566, 2015.
- Lund-Hansen, L. C., Andersen, T. J., Nielsen, M. H., and Pejrup, M.: Suspended Matter, Chl-a, CDOM, Grain Sizes, and Optical Properties in the Arctic Fjord-Type Estuary, Kangerlussuaq, West Greenland During Summer, *Estuaries and Coasts*, 33, 1442–1451, <https://doi.org/10.1007/S12237-010-9300-7/FIGURES/5>, 2010.
- Luo, H., Castelao, R. M., Rennermalm, A. K., Tedesco, M., Bracco, A., Yager, P. L., and Mote, T. L.: Oceanic transport of surface meltwater from the southern Greenland ice sheet, *Nat Geosci*, 9, 528–532, <https://doi.org/10.1038/ngeo2708>, 2016.
- Marín, V. H., Tironi, A., Paredes, M. A., and Contreras, M.: Modeling suspended solids in a Northern Chilean Patagonia glacier-fed fjord: GLOF scenarios under climate change conditions, *Ecol Modell*, 264, 7–16, <https://doi.org/10.1016/j.ecolmodel.2012.06.017>, 2013.
- McGovern, M., Pavlov, A. K., Deininger, A., Granskog, M. A., Leu, E., Søreide, J. E., and Poste, A. E.: Terrestrial Inputs Drive Seasonality in Organic Matter and Nutrient Biogeochemistry in a High Arctic Fjord System (Isfjorden, Svalbard), *Front Mar Sci*, 7, 747, <https://doi.org/10.3389/fmars.2020.542563>, 2020.
- Mckinney, W.: *Data Structures for Statistical Computing in Python*, 2010.
- Meire, L., Sjøgaard, D. H., Mortensen, J., Meysman, F. J. R., Soetaert, K., Arendt, K. E., Juul-Pedersen, T., Blicher, M. E., and Rysgaard, S.: Glacial meltwater and primary production are drivers of strong CO₂ uptake in fjord and coastal waters adjacent to the Greenland Ice Sheet, *Biogeosciences*, 12, 2347–2363, <https://doi.org/10.5194/bg-12-2347-2015>, 2015.
- Meire, L., Mortensen, J., Meire, P., Juul-Pedersen, T., Sejr, M. K., Rysgaard, S., Nygaard, R., Huybrechts, P., and Meysman, F. J. R.: Marine-terminating glaciers sustain high productivity in Greenland fjords, *Glob Chang Biol*, 23, 5344–5357, <https://doi.org/10.1111/gcb.13801>, 2017.
- Milner, A. M., Khamis, K., Battin, T. J., Brittain, J. E., Barrand, N. E., Füreder, L., Cauvy-Fraunié, S., Gíslason, G. M., Jacobsen, D., Hannah, D. M., Hodson, A. J., Hood, E., Lencioni, V., Ólafsson, J. S., Robinson, C. T., Tranter, M., and Brown, L. E.: Glacier shrinkage driving global changes in downstream systems, <https://doi.org/10.1073/pnas.1619807114>, 12 September 2017.
- Møller, E. F., Christensen, A., Larsen, J., Mankoff, K. D., Ribergaard, M. H., Sejr, M., Wallhead, P., and Maar, M.: The sensitivity of primary productivity in Disko Bay, a coastal Arctic ecosystem, to changes in freshwater discharge and sea ice cover, *Ocean Sci*, 19, 403–420, <https://doi.org/10.5194/os-19-403-2023>, 2023.
- Moskalik, M., Tegowski, J., Grabowiecki, P., and Zulichowska, M.: Principal component and cluster analysis for determining diversification of bottom morphology based on bathymetric profiles from Brepollen (Hornsund, Spitsbergen), *Oceanologia*, 56, 59–84, <https://doi.org/10.5697/oc.56-1.059>, 2014.

- Moskalik, M., Cwiąkała, J., Szczuciński, W., Dominiczak, A., Głowacki, O., Wojtysiak, K., and Zagórski, P.: Spatiotemporal changes in the concentration and composition of suspended particulate matter in front of Hansbreen, a tidewater glacier in Svalbard, *Oceanologia*, 60, 446–463, <https://doi.org/10.1016/j.oceano.2018.03.001>, 2018.
- Muckenhuber, S., Nilsen, F., Korosov, A., and Sandven, S.: Sea ice cover in Isfjorden and Hornsund, Svalbard (2000–2014) from remote sensing data, *Cryosphere*, 10, 149–158, <https://doi.org/10.5194/tc-10-149-2016>, 2016.
- 750 Mugford, R. I. and Dowdeswell, J. A.: Modeling iceberg-rafted sedimentation in high-latitude fjord environments, *J Geophys Res*, 115, F03024, <https://doi.org/10.1029/2009JF001564>, 2010.
- Mugford, R. I. and Dowdeswell, J. A.: Modeling glacial meltwater plume dynamics and sedimentation in high-latitude fjords, *J Geophys Res Earth Surf*, 116, n/a-n/a, <https://doi.org/10.1029/2010JF001735>, 2011.
- 755 Neder, C., Fofonova, V., Androsov, A., Kuznetov, I., Abele, D., Falk, U., Schloss, I. R., Sahade, R., and Jerosch, K.: Modelling suspended particulate matter dynamics at an Antarctic fjord impacted by glacier melt, *Journal of Marine Systems*, 103734, <https://doi.org/10.1016/j.jmarsys.2022.103734>, 2022.
- Nowak, A., Hodgkins, R., Nikulina, A., Osuch, M., Wawrzyniak, T., Kavan, J., Łepkowska, E., Majerska, M., Romashova, K., Vasilevich, I., Sobota, I., & Rachlewicz, G.: From land to fjords: The review of Svalbard hydrology from 1970 to 2019 (SvalHydro). In SESS report 2020 - The State of Environmental Science in Svalbard - an annual report (pp. 176–201). Svalbard Integrated Arctic Earth Observing System. <https://doi.org/10.5281/zenodo.4294063>, 2020.
- 760 Oliver, H., Castelao, R. M., Wang, C., and Yager, P. L.: Meltwater-Enhanced Nutrient Export From Greenland’s Glacial Fjords: A Sensitivity Analysis, *J Geophys Res Oceans*, 125, e2020JC016185, <https://doi.org/10.1029/2020JC016185>, 2020.
- Osika, A., Jania, J., and Szafraniec, J. E.: Holocene ice-free strait followed by dynamic Neoglacial fluctuations: Hornsund, Svalbard, *Holocene*, 32, 664–679, <https://doi.org/10.1177/09596836221088232>, 2022.
- 765 Overeem, I., Hudson, B. D., Syvitski, J. P. M., Mikkelsen, A. B., Hasholt, B., Van Den Broeke, M. R., Noel, B. P. Y., and Morlighem, M.: Substantial export of suspended sediment to the global oceans from glacial erosion in Greenland, *Nat Geosci*, 10, 859–863, <https://doi.org/10.1038/NNGEO3046>, 2017.
- Pasculli, L., Piermattei, V., Madonia, A., Bruzzone, G., Caccia, M., Ferretti, R., Odetti, A., and Marcelli, M.: New Cost-Effective Technologies Applied to the Study of the Glacier Melting Influence on Physical and Biological Processes in Kongsfjorden Area (Svalbard), *J Mar Sci Eng*, 8, 593, <https://doi.org/10.3390/jmse8080593>, 2020.
- 770 Peck, L. S., Barnes, D. K. A., Cook, A. J., Fleming, A. H., and Clarke, A.: Negative feedback in the cold: Ice retreat produces new carbon sinks in Antarctica, *Glob Chang Biol*, 16, 2614–2623, <https://doi.org/10.1111/j.1365-2486.2009.02071.x>, 2010.
- Van Pelt, W., Pohjola, V., Pettersson, R., Marchenko, S., Kohler, J., Luks, B., Ove Hagen, J., Schuler, T. V., Dunse, T., Noël, B., and Reijmer, C.: A long-term dataset of climatic mass balance, snow conditions, and runoff in Svalbard (1957–2018), *Cryosphere*, 13, 2259–2280, <https://doi.org/10.5194/tc-13-2259-2019>, 2019.
- 775 Pfannkuche, J. and Schmidt, A.: Determination of suspended particulate matter concentration from turbidity measurements: particle size effects and calibration procedures, *Hydrol Process*, 17, 1951–1963, <https://doi.org/10.1002/HYP.1220>, 2003.

- Pfeffer, W. T., Arendt, A. A., Bliss, A., Bolch, T., Cogley, J. G., Gardner, A. S., Hagen, J. O., Hock, R., Kaser, G., Kienholz, C., Miles, E. S., Moholdt, G., Mölg, N., Paul, F., Radić, V., Rastner, P., Raup, B. H., Rich, J., Sharp, M. J., Andreassen, L. M., Bajracharya, S., Barrand, N. E., Beedle, M. J., Berthier, E., Bhambri, R., Brown, I., Burgess, D. O., Burgess, E. W., Cawkwell, F., Chinn, T., Copland, L., Cullen, N. J., Davies, B., De Angelis, H., Fountain, A. G., Frey, H., Giffen, B. A., Glasser, N. F., Gurney, S. D., Hagg, W., Hall, D. K., Haritashya, U. K., Hartmann, G., Herreid, S., Howat, I., Jiskoot, H., Khromova, T. E., Klein, A., Kohler, J., König, M., Kriegel, D., Kutuzov, S., Lavrentiev, I., Le Bris, R., Li, X., Manley, W. F., Mayer, C., Menounos, B., Mercer, A., Mool, P., Negrete, A., Nosenko, G., Nuth, C., Osmonov, A., Pettersson, R., Racoviteanu, A., Ranzi, R., Sarikaya, M. A., Schneider, C., Sigurdsson, O., Sirguey, P., Stokes, C. R., Wheate, R., Wolken, G. J., Wu, L. Z., and Wyatt, F. R.: The randolph glacier inventory: A globally complete inventory of glaciers, *Journal of Glaciology*, 60, 537–552, <https://doi.org/10.3189/2014JoG13J176>, 2014.
- Piwoz, K., Walkusz, W., Hapter, R., Wiczorek, P., Hop, H., and Wiktor, J.: Comparison of productivity and phytoplankton in a warm (Kongsfjorden) and a cold (Hornsund) Spitsbergen fjord in mid-summer 2002, *Polar Biol*, 32, 549–559, <https://doi.org/10.1007/s00300-008-0549-2>, 2009.
- Platt, T., Harrison, W. G., Irwin, B., Horne, E. P., and Gallegos, C. L.: Photosynthesis and photoadaptation of marine phytoplankton in the arctic, *Deep Sea Research Part A. Oceanographic Research Papers*, 29, 1159–1170, [https://doi.org/10.1016/0198-0149\(82\)90087-5](https://doi.org/10.1016/0198-0149(82)90087-5), 1982.
- Van De Poll, W. H., Kulk, G., Rozema, P. D., Brussaard, C. P. D., Visser, R. J. W., and Buma, A. G. J.: Contrasting glacial meltwater effects on post-bloom phytoplankton on temporal and spatial scales in Kongsfjorden, Spitsbergen, *Elementa*, 6, <https://doi.org/10.1525/ELEMENTA.307/112827>, 2018.
- Promińska, A., Cisek, M., and Walczowski, W.: Kongsfjorden and Hornsund hydrography – comparative study based on a multiyear survey in fjords of west Spitsbergen, *Oceanologia*, 59, 397–412, <https://doi.org/10.1016/j.oceano.2017.07.003>, 2017.
- Reback, J., McKinney, W., jbrockmendel, Bossche, J. Van den, Augspurger, T., Cloud, P., gyoung, Sinhrks, Klein, A., Hawkins, S., Roeschke, M., Tratner, J., She, C., Ayd, W., Petersen, T., MomIsBestFriend, Garcia, M., Schendel, J., Hayden, A., Jancauskas, V., Battiston, P., Saxton, D., Seabold, S., alimcmaster1, chris-b1, h-vetinari, Hoyer, S., Dong, K., Overmeire, W., and Winkel, M.: pandas-dev/pandas: Pandas 1.0.5, <https://doi.org/10.5281/ZENODO.3898987>, 2020.
- Rignot, E., Box, J. E., Burgess, E., and Hanna, E.: Mass balance of the Greenland ice sheet from 1958 to 2007, *Geophys Res Lett*, 35, L20502, <https://doi.org/10.1029/2008GL035417>, 2008.
- Van Rossum, G. and Drake, F. L.: *Python 3 Reference Manual*, 2009.
- Ruben, M., Hefter, J., Schubotz, F., Geibert, W., Butzin, M., Gentz, T., Grotheer, H., Forwick, M., Szczuciński, W., and Mollenhauer, G.: Fossil organic carbon utilization in marine Arctic fjord sediments by subsurface micro-organisms, *Nature Geoscience* 2023 16:7, 16, 625–630, <https://doi.org/10.1038/s41561-023-01198-z>, 2023.
- Sagan, S. and Darecki, M.: Inherent optical properties and particulate matter distribution in summer season in waters of Hornsund and Kongsfjordenen, Spitsbergen, *Oceanologia*, 60, 65–75, <https://doi.org/10.1016/j.oceano.2017.07.006>, 2018.

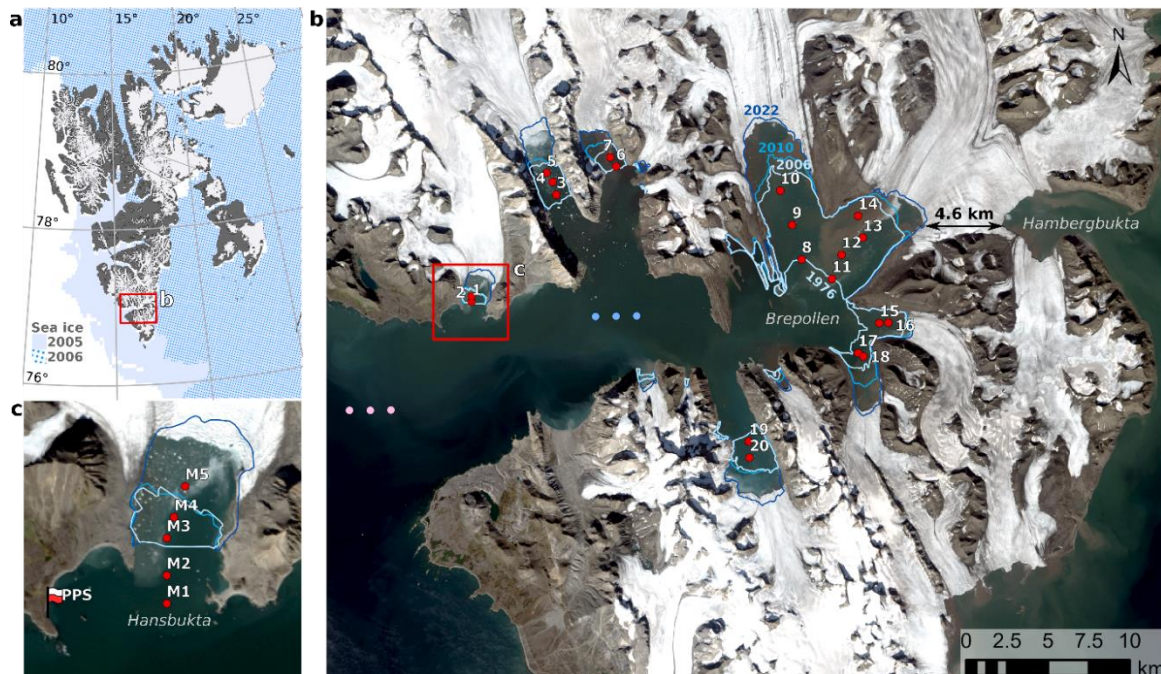
- dos Santos, T. D., Barnes, J. M., Goldberg, D. N., Gudmundsson, G. H., and Morlighem, M.: Drivers of Change of Thwaites Glacier, West Antarctica, Between 1995 and 2015, *Geophys Res Lett*, 48, e2021GL093102, <https://doi.org/10.1029/2021GL093102>, 2021.
- 815 Schofield, O., Ducklow, H. W., Martinson, D. G., Meredith, M. P., Moline, M. A., and Fraser, W. R.: How do polar marine ecosystems respond to rapid climate change?, <https://doi.org/10.1126/science.1185779>, 18 June 2010.
- Simo-Matchim, A. G., Gosselin, M., Blais, M., Gratton, Y., and Tremblay, J. É.: Seasonal variations of phytoplankton dynamics in Nunatsiavut fjords (Labrador, Canada) and their relationships with environmental conditions, *Journal of Marine Systems*, 156, 56–75, <https://doi.org/10.1016/J.JMARSYS.2015.11.007>, 2016.
- 820 Smith, R. W., Bianchi, T. S., Allison, M., Savage, C., and Galy, V.: High rates of organic carbon burial in fjord sediments globally, *Nat Geosci*, 8, 450–453, <https://doi.org/10.1038/NGEO2421>, 2015.
- Steiner, N., Deal, C., Lannuzel, D., Lavoie, D., Massonnet, F., Miller, L. A., Moreau, S., Popova, E., Stefels, J., and Tedesco, L.: What sea-ice biogeochemical modellers need from observers, *Elementa*, 2016, 84, <https://doi.org/10.12952/journal.elementa.000084>, 2016.
- 825 Strom, S. L., Fredrickson, K. A., and Bright, K. J.: Spring phytoplankton in the eastern coastal Gulf of Alaska: Photosynthesis and production during high and low bloom years, *Deep Sea Research Part II: Topical Studies in Oceanography*, 132, 107–121, <https://doi.org/10.1016/J.DSR2.2015.05.003>, 2016.
- Strzelecki, M. C., Szczuciński, W., Dominiczak, A., Zagórski, P., Dudek, J., and Knight, J.: New fjords, new coasts, new landscapes: The geomorphology of paraglacial coasts formed after recent glacier retreat in Brepollen (Hornsund, southern
- 830 Svalbard), *Earth Surf Process Landf*, 45, 1325–1334, <https://doi.org/10.1002/esp.4819>, 2020.
- Stuart, V., Sathyendranath, S., Head, E. J. H., Platt, T., Irwin, B., and Maass, H.: Bio-optical characteristics of diatom and prymnesiophyte populations in the Labrador Sea, *Mar Ecol Prog Ser*, 201, 91–106, <https://doi.org/10.3354/MEPS201091>, 2000.
- Sutherland, D. A., Straneo, F., Stenson, G. B., Davidson, F. J. M., Hammill, M. O., and Rosing-Asvid, A.: Atlantic water
- 835 variability on the SE Greenland continental shelf and its relationship to SST and bathymetry, *J Geophys Res Oceans*, 118, 847–855, <https://doi.org/10.1029/2012JC008354>, 2013.
- Syvitski, J., Vörösmarty, C. J., Kettner, A. J., and Green, P.: Impact of Humans on the Flux of Terrestrial Sediment to the Global Coastal Ocean, *Science (1979)*, 308, 376–380, <https://doi.org/10.1126/science.1109454>, 2005.
- Syvitski, J., Ángel, J. R., Saito, Y., Overeem, I., Vörösmarty, C. J., Wang, H., and Olago, D.: Earth’s sediment cycle during
- 840 the Anthropocene, *Nat Rev Earth Environ*, 3, 179–196, <https://doi.org/10.1038/s43017-021-00253-w>, 2022.
- Szczuciński, W., Zajaczkowski, M., and Scholten, J.: Sediment accumulation rates in subpolar fjords - Impact of post-Little Ice Age glaciers retreat, *Billefjorden, Svalbard, Estuar Coast Shelf Sci*, 85, 345–356, <https://doi.org/10.1016/j.ecss.2009.08.021>, 2009.
- Szeligowska, M., Trudnowska, E., Boehnke, R., Dąbrowska, A. M., Dragańska-Deja, K., Deja, K., Darecki, M., and
- 845 Błachowiak-Samołyk, K.: The interplay between plankton and particles in the Isfjorden waters influenced by marine- and

- land-terminating glaciers, *Science of the Total Environment*, 780, 146491, <https://doi.org/10.1016/j.scitotenv.2021.146491>, 2021.
- Szeligowska, M., Trudnowska, E., Boehnke, R., and Błachowiak-Samołyk, K.: Dark plumes of glacial meltwater affect vertical distribution of zooplankton in the Arctic, *Sci Rep*, 12, 17953, <https://doi.org/10.1038/s41598-022-22475-8>, 2022.
- 850 Torsvik, T., Albreetsen, J., Sundfjord, A., Kohler, J., Sandvik, A. D., Skarðhamar, J., Lindbäck, K., and Everett, A.: Impact of tidewater glacier retreat on the fjord system: Modeling present and future circulation in Kongsfjorden, Svalbard, *Estuar Coast Shelf Sci*, 220, 152–165, <https://doi.org/10.1016/j.ecss.2019.02.005>, 2019.
- Van Pelt, W. J., Schuler, T. V., Pohjola, V. A., & Pettersson, R.: Accelerating future mass loss of Svalbard glaciers from a multi-model ensemble. *Journal of Glaciology*, 67(263), 485–499, <https://doi.org/10.1017/jog.2021.2>, 2021.
- 855 Vonnahme, T. R., Persson, E., Dietrich, U., Hejdukova, E., Dybwad, C., Elster, J., Chierici, M., and Gradinger, R.: Early spring subglacial discharge plumes fuel under-ice primary production at a Svalbard tidewater glacier, *Cryosphere*, 15, 2083–2107, <https://doi.org/10.5194/tc-15-2083-2021>, 2021.
- Wadham, J. L., Hawkings, J. R., Tarasov, L., Gregoire, L. J., Spencer, R. G. M., Gutjahr, M., Ridgwell, A., and Kohfeld, K. E.: Ice sheets matter for the global carbon cycle, <https://doi.org/10.1038/s41467-019-11394-4>, 1 December 2019.
- 860 Walch, D. M. R., Singh, R. K., Søreide, J. E., Lantuit, H., and Poste, A.: Spatio-Temporal Variability of Suspended Particulate Matter in a High-Arctic Estuary (Adventfjorden, Svalbard) Using Sentinel-2 Time-Series, <https://doi.org/10.3390/rs14133123>, 2022.
- Wawrzyniak, T. and Osuch, M.: A 40-year High Arctic climatological dataset of the Polish Polar Station Hornsund (SW Spitsbergen, Svalbard), *Earth Syst Sci Data*, 12, 805–815, <https://doi.org/10.5194/essd-12-805-2020>, 2020.
- 865 Węśławski, J. M., Buchholz, F., Głuchowska, M., and Weydmann, A.: Ecosystem maturation follows the warming of the Arctic fjords, *Oceanologia*, 59, 592–602, <https://doi.org/10.1016/j.oceano.2017.02.002>, 2017.
- Riser, C. W., Wassmann, P., Reigstad, M., and Seuthe, L.: Vertical flux regulation by zooplankton in the northern Barents Sea during Arctic spring, *Deep Sea Res 2 Top Stud Oceanogr*, 55, 2320–2329, <https://doi.org/10.1016/j.dsr2.2008.05.006>, 2008.
- 870 Włodarska-Kowalczyk, M., Mazurkiewicz, M., Górska, B., Michel, L. N., Jankowska, E., and Zaborska, A.: Organic Carbon Origin, Benthic Faunal Consumption, and Burial in Sediments of Northern Atlantic and Arctic Fjords (60–81°N), *J Geophys Res Biogeosci*, 124, 3737–3751, <https://doi.org/10.1029/2019JG005140>, 2019.
- Wöfl, A. C., Lim, C. H., Hass, H. C., Lindhorst, S., Tosonotto, G., Lettmann, K. A., Kuhn, G., Wolff, J. O., and Abele, D.: Distribution and characteristics of marine habitats in a subpolar bay based on hydroacoustics and bed shear stress estimates—Potter Cove, King George Island, Antarctica, *Geo-Marine Letters*, 34, 435–446, <https://doi.org/10.1007/s00367-014-0375-1>, 2014.
- 875 Yumruktepe, V. Ç., Samuelsen, A., and Daewel, U.: ECOSMO II(CHL): a marine biogeochemical model for the North Atlantic and the Arctic, *Geosci Model Dev*, 15, 3901–3921, <https://doi.org/10.5194/gmd-15-3901-2022>, 2022.

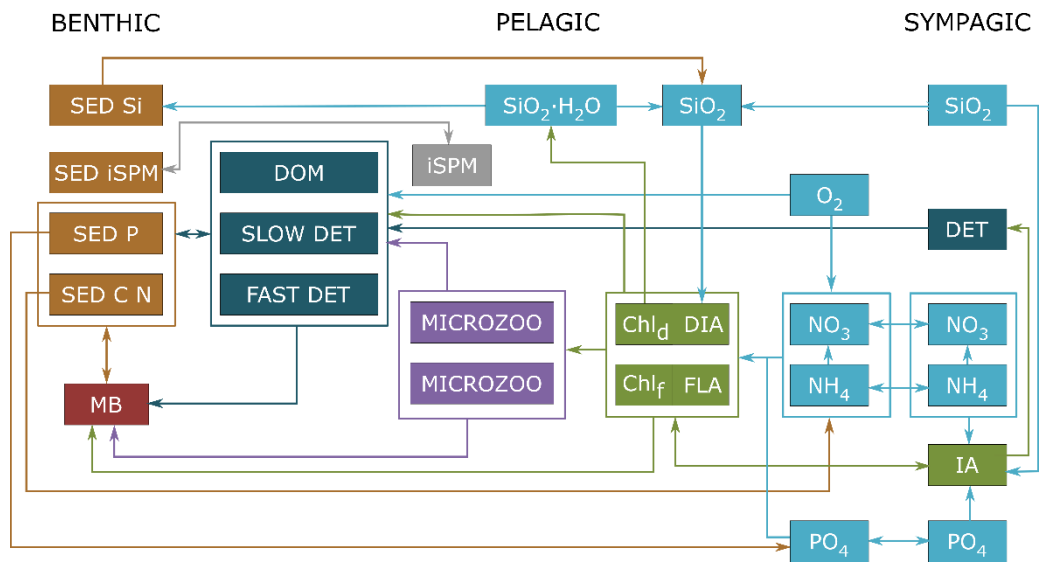
Zaborska, A., Włodarska-Kowalczyk, M., Legeżyńska, J., Jankowska, E., Winogradow, A., and Deja, K.: Sedimentary organic matter sources, benthic consumption and burial in west Spitsbergen fjords – Signs of maturing of Arctic fjordic systems?, *Journal of Marine Systems*, 180, 112–123, <https://doi.org/10.1016/j.jmarsys.2016.11.005>, 2018.

Zwerschke, N., Sands, C. J., Roman-Gonzalez, A., Barnes, D. K. A., Guzzi, A., Jenkins, S., Muñoz-Ramírez, C., and Scourse, J.: Quantification of blue carbon pathways contributing to negative feedback on climate change following glacier retreat in West Antarctic fjords, *Glob Chang Biol*, 28, 8–20, <https://doi.org/10.1111/gcb.15898>, 2022.

885

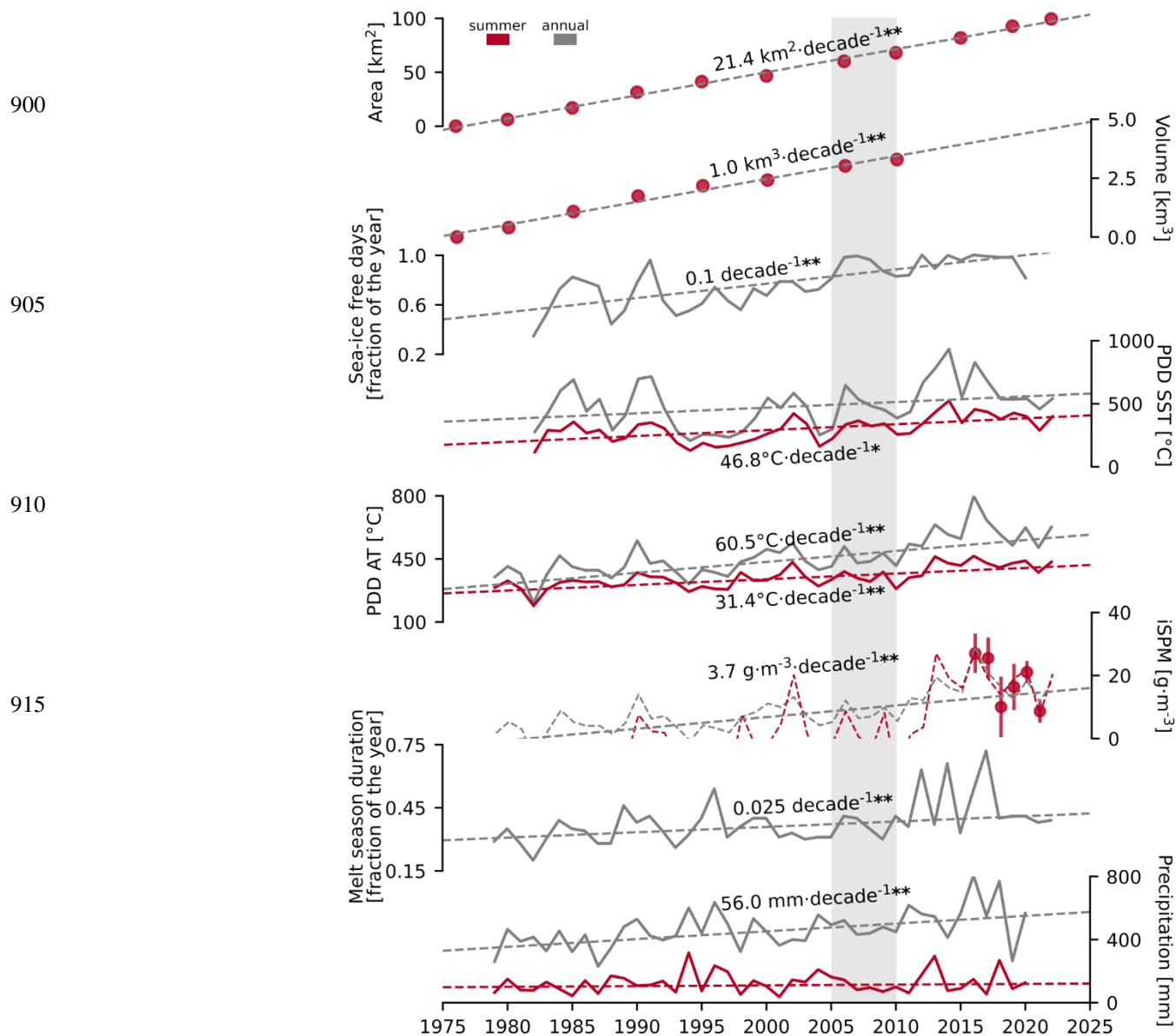


890 **Figure 1:** a) Svalbard archipelago with monthly mean sea-ice extent (SIC>15%) in March 2005 (plain colour) and 2006 (dotted). Land and glaciers extent downloaded from <https://geodata.npolar.no/>. The red frame indicates the location of Hornsund. b) Newly-ice-free areas in Hornsund which have opened since 1976 (blue lines – glaciers' front position in 1976, 2006, 2010, and 2022) with the width of the ice bridge between Brepollen and Hambergbukta. The dots indicate modelled stations (1-20, red), and three data points for SST (pink) and SI (blue) each. The red frame indicates the location of Hansbukta. c) Long-term SPM and sediment flux monitoring stations in Hansbukta (M1-5, red dots) and Polish Polar Station Hornsund (PPS). Landsat8 satellite image (04/08/2020) downloaded from <https://glovis.usgs.gov/app>.

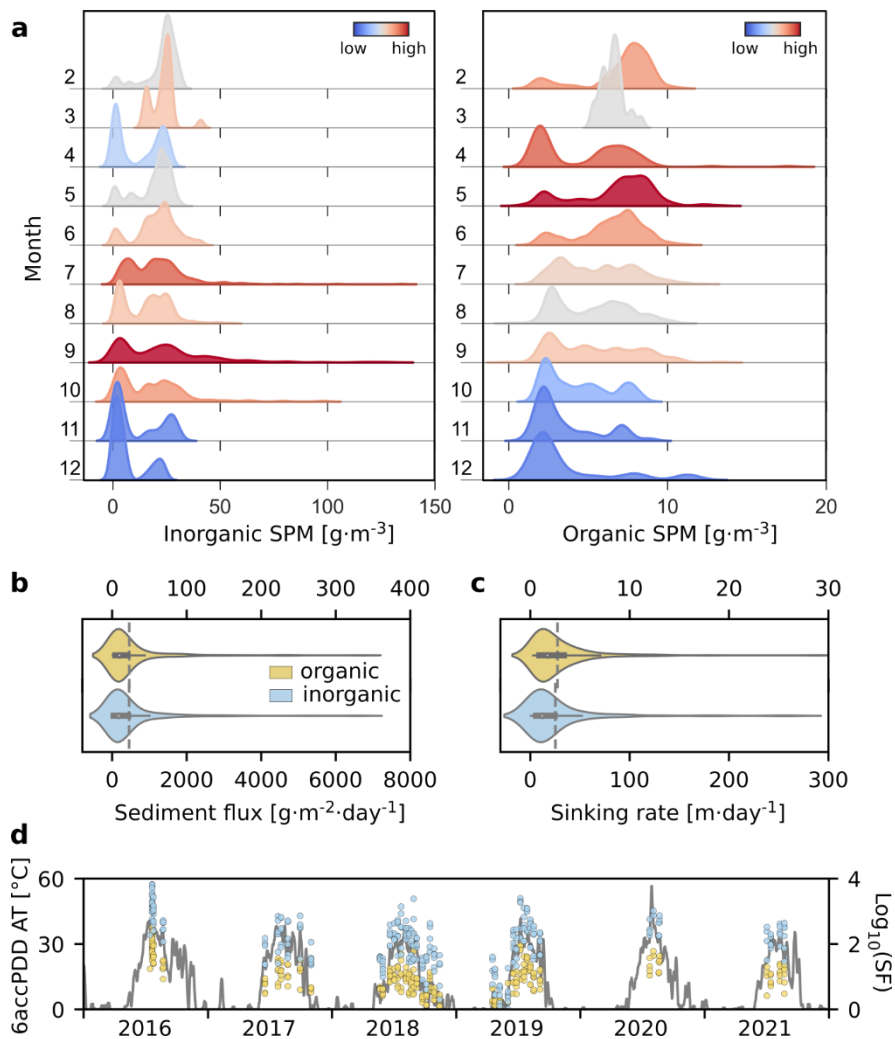


895

Figure 2: Schematic diagram of the biogeochemical model ECOSMO-E2E-Polar with new iSPM group. The three systems (benthic, pelagic, and sympagic) are included.



920 **Figure 3: Long-term trends in the newly ice-free marine habitat and melt potential in Hornsund. Area (km²) and volume (km³) of newly ice-free marine habitat (assessed for summers between 1976 and 2022), sea ice-free days (fraction of the year, 1982-2020), accumulated positive degree days for sea surface temperature and air (PDD SST and PDD AT, °C, 1979-2022), inorganic SPM concentration reconstructed from 6 years of monitoring (g·m⁻³, 1979-2022), melt season duration (fraction of the year, 1979-2022), and precipitation (mm, 1979-2020). * p<0.05, **p<0.001 for modified Mann-Kendal test. Grey shading indicates the modelling period (2005-2009).**



925 **Figure 4: SPM dynamics at monitoring stations in Hansbutka in 2016-2021. a) Kernel density estimates of SPM concentration ($\text{g}\cdot\text{m}^{-3}$, inorganic - left, organic - right). Colours indicate the distribution between months (high to low) b) Inorganic (blue) and organic (yellow) sediment flux ($\text{g}\cdot\text{m}^{-2}\cdot\text{day}^{-1}$, grey dashed line - mean value). c) Inorganic and organic matter sinking rate ($\text{m}\cdot\text{day}^{-1}$, grey dashed line - mean value). d) inorganic and organic sediment flux (SF, dots, log scale) and accumulated daily air temperature for positive degree days for 6 days window ($^{\circ}\text{C}$, 6accPDD AT, line).**

930

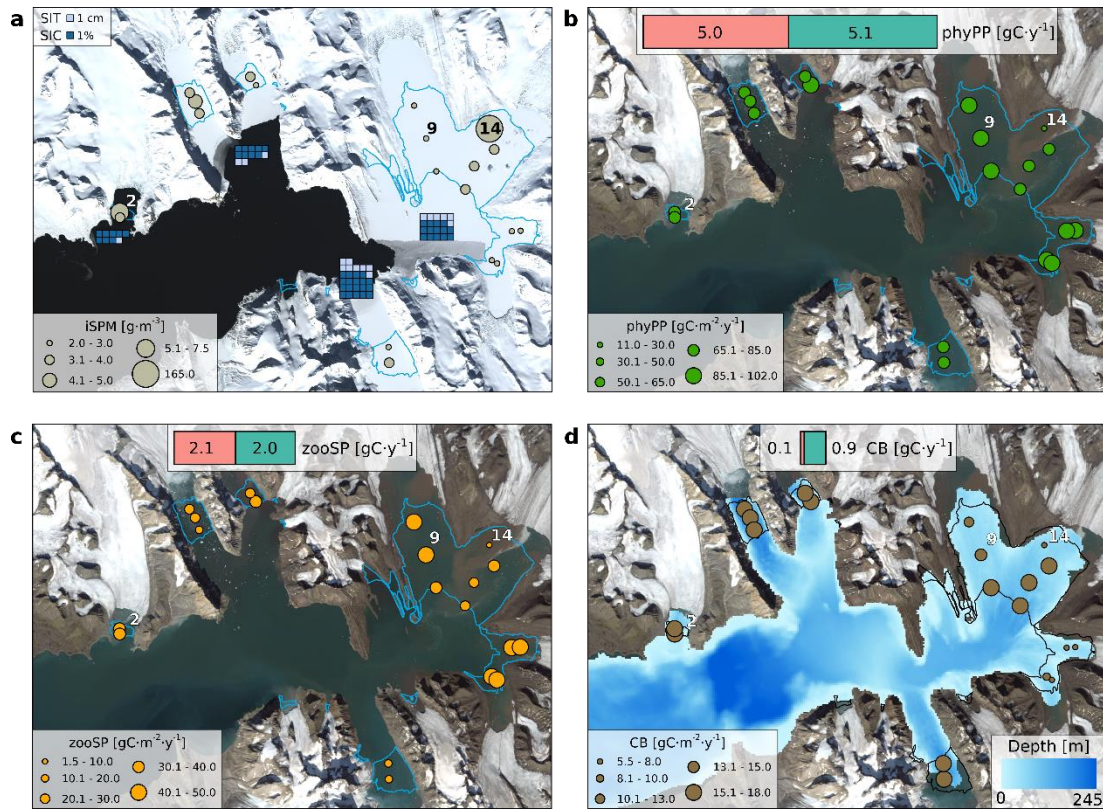
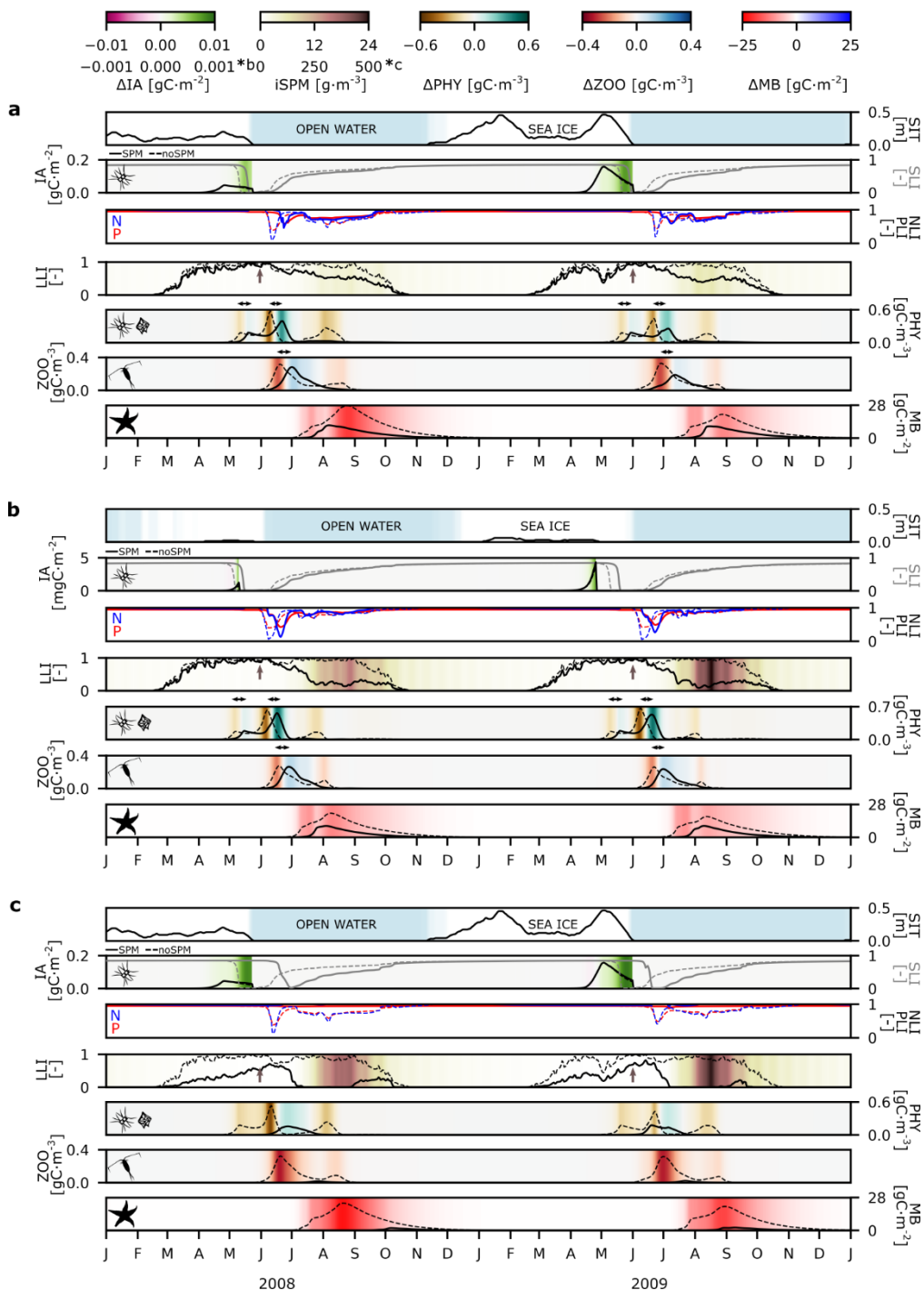


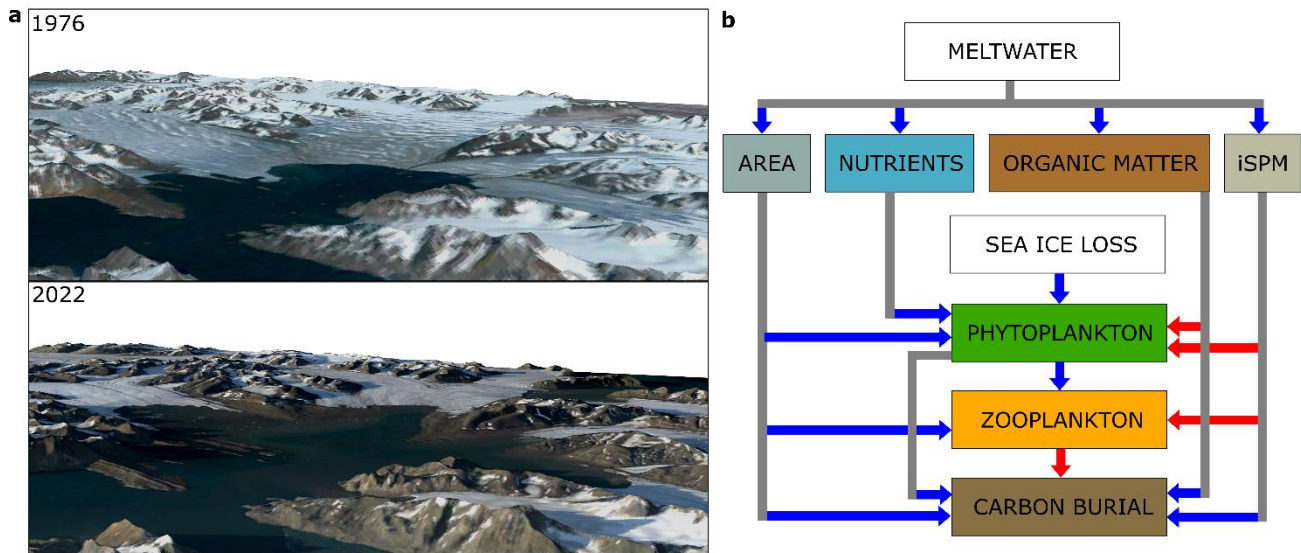
Figure 5: Spatial patterns in average sea ice thickness (SIT, cm) and concentration (SIC, %) in May, summertime integrated inorganic SPM concentration (iSPM, $\text{g}\cdot\text{m}^{-3}$) (a), plankton primary (b) and secondary (c) production (phyPP, zooSP), and carbon burial (d, CB) ($\text{gC}\cdot\text{m}^{-2}\cdot\text{y}^{-1}$) with blue carbon gains due to the retreat of marine-terminating glaciers (green, SPM scenario) and losses due to the inorganic SPM discharge with meltwater (pink, noSPM-SPM scenario, GgC per year, average for 2005-2009). The lines indicate newly ice-free areas extent in 2006. Ecosystem dynamics at stations 2, 9, and 14 is presented in Fig. 6. Landsat8 satellite images (a - 14/05/2022 and b, c, d - 04/08/2020) downloaded from <https://glovis.usgs.gov/app>.

935



940 **Figure 6: Changes in ecosystem dynamics due to iSPM input in 2008 and 2009 at three modelled stations: a – low iSPM influence (station 9), b – medium iSPM influence (station 2), c – high iSPM influence (station 14). Line plots show sea ice thickness (SIT, m), the biomass of ice algae (IA, $\text{gC}\cdot\text{m}^{-2}$ or $\text{mgC}\cdot\text{m}^{-2}$, black), integrated silicate (grey), phosphorus (red), nitrogen (blue) and light limitation index (SLI, PLI, NLI, LLI, -), integrated biomass of phytoplankton and zooplankton (PHY and ZOO, $\text{gC}\cdot\text{m}^{-3}$), and**

945 macrobenthos biomass (MB, $\text{gC}\cdot\text{m}^{-2}$). Full line – SPM scenario, dashed line – noSPM scenario. SLI and LLI equal to 1 indicate that phytoplankton is not limited either by silicate or light. Colour plots indicate the SIC<15% (blue, open water), differences in ice algae, phytoplankton, zooplankton and macrobenthos biomass between SPM and noSPM scenario (SPM-noSPM), and integrated inorganic SPM concentration in the SPM scenario (iSPM, $\text{g}\cdot\text{m}^{-3}$). Brown arrows indicate the start of the melt season (30th of May 2008 and 3rd of June 2009) and black arrows indicate delays in peak abundance of phytoplankton and zooplankton. Note the different scales (*).



950 **Figure 7:** a) 3D representation of the inner Hornsund bay (Brepollen) in the summer of 1976 and 2022. Landsat satellite images (18/07/1976 and 15/08/2022) were downloaded from <https://glovis.usgs.gov/app>. Digital elevation model data were downloaded from <https://arcticdem.apps.pgc.umn.edu/>. b) Schematic representation of the positive (blue arrows) and negative (red arrows) feedback mechanisms influencing biological production and carbon burial in the Arctic fjords.

Table 1 Sources of the input data and modelling setup

Variable	Data source	Data point	Glacial bay	Coordinates (°N, °E)	Depth (m)
Temperature and salinity	numerical model of Hornsund (HRM) (Jakacki et al., 2017)	H1_08	Hansbukta	77.009, 15.624	37.87
		HH1		77.012, 15.624	42.45
		BuP1_05	Vestre	77.067, 15.834	97.29
		HA2	Burgerbukta	77.074, 15.825	61.79
		HA3		77.079, 15.811	61.06
		HA0	Austre	77.082, 15.981	57.71
		HA1	Burgerbukta	77.087, 15.967	76.93
		BrS1_02	Brepollen	77.029, 16.431	55.13
		BrS1_03		77.048, 16.409	47.35
		HB2		77.067, 16.382	44.62
		H3	Brepollen	77.018, 16.503	88.02
		BrH1_03		77.031, 16.528	76.32
		BrH1_04		77.040, 16.581	55.45
		HB1		77.052, 16.571	49.55
		BrSv1_04	Telegrafbukta	77.040, 16.581	32.81
		HM2		76.993, 16.638	28.46
		BrM1_04	Mendeleevbukta	76.977, 16.562	38.97
		HM1		76.975, 16.575	32.65
HS2	Samarinvågen	76.930, 16.292	103.07		
HS1		76.921, 16.292	98.72		
Sea ice concentration and thickness	S800 model (Albretsen et al., 2017)	H1_08, HH1 (1-2) BuP1_05, HA2, HA3, HA0, HA1 (3-7) BrS1_02, BrS1_03, HB2, H3, BrH1_03, BrH1_04, HB1, BrSv1_04, HM2, BrM1_04, HM1 (8-18) HS1, HS2 (19-20)		77.003, 15.637 77.037, 16.022 76.993, 16.369 76.965, 16.239	
Meteorological data	Polish Polar Station Hornsund	PPS		77.000, 15.550	
BGC tracers	mean values from the literature				
Modelling setup					
Model	1D GOTM-ECOSMO-E2E-Polar		Simulation time	01/01/2005 – 31/12/2009	
Spin up	5 years (2005-2009 average)		Time step	30 min	
Depth layers	20		Output	daily average	

Table 2 List of parameters, corresponding description, and units used in the model.

Abbreviation	Definition	Value	Units
τ_{crit}	Critical bottom shear stress	0.07	$\text{N}\cdot\text{m}^{-2}$
λ_{d2s}	Sedimentation rate if $\tau < \tau_{crit}$	3.5	$\text{m}\cdot\text{day}^{-1}$
λ_{s2d}	Resuspension rate if $\tau \geq \tau_{crit}$	26	day^{-1}
w_D	Inorganic SPM sinking rate	0.8	$\text{m}\cdot\text{day}^{-1}$
k_w	Water extinction coefficient	0.05	m^{-1}
k_{Chl}	Chlorophyll <i>a</i> extinction coefficient	0.2	$\text{m}^2(\text{m}\cdot\text{molC})^{-1}$
k_{iSPM}	Inorganic SPM light extinction coefficient	0.065	m^2g^{-1}
k_{DOM}	Dissolved organic matter light extinction coefficient	0.29	$\text{m}^2(\text{m}\cdot\text{molC})^{-1}$
a	Photosynthesis efficiency parameter	0.04	$(\text{W}\cdot\text{m}^{-2})^{-1}$
m_{MB}	Macrobenthos mortality rate	0.03	day^{-1}
δ_{bur}	Burial rate	0.0	day^{-1}
η_{bur}	Burial efficiency	0.7	-